Cellular and Molecular Life Sciences (2023) 80:255
https://doi.org/10.1007/s00018-023-04895-5

ORIGINAL ARTICLE

RGS7 balances acetylation/de-acetylation of p65 to control chemotherapy-dependent cardiac inflammation

Madhuri Basak[1] · Kiran Das[1] · Tarun Mahata[1] · Dinesh Kumar[1] · Nupur Nagar[2] · Krishna Mohan Poluri[2] · Pranesh Kumar[3] · Priyadip Das[4] · Adele Stewart[5] · Biswanath Maity[1]

Received: 17 April 2023 / Revised: 28 June 2023 / Accepted: 22 July 2023 / Published online: 17 August 2023

Abstract

Cardiotoxicity remains a major limitation in the clinical utility of anthracycline chemotherapeutics. Regulator of G-protein Signaling 7 (RGS7) and inflammatory markers are up-regulated in the hearts of patients with a history of chemotherapy particularly those with reduced left-ventricular function. RGS7 knockdown in either the murine myocardium or isolated murine ventricular cardiac myocytes (VCM) or cultured human VCM provided marked protection against doxorubicin-dependent oxidative stress, NF-κB activation, inflammatory cytokine production, and cell death. In exploring possible mechanisms causally linking RGS7 to pro-inflammatory signaling cascades, we found that RGS7 forms a complex with acetylase Tip60 and deacetylase sirtuin 1 (SIRT1) and controls the acetylation status of the p65 subunit of NF-κB. In VCM, the detrimental impact of RGS7 could be mitigated by inhibiting Tip60 or activating SIRT1, indicating that the ability of RGS7 to modulate cellular acetylation capacity is critical for its pro-inflammatory actions. Further, RGS7-driven, Tip60/SIRT1-dependent cytokines released from ventricular cardiac myocytes and transplanted onto cardiac fibroblasts increased oxidative stress, markers of transdifferentiation, and activity of extracellular matrix remodelers emphasizing the importance of the RGS7–Tip60–SIRT1 complex in paracrine signaling in the myocardium. Importantly, while RGS7 overexpression in heart resulted in sterile inflammation, fibrotic remodeling, and compromised left-ventricular function, activation of SIRT1 counteracted the detrimental impact of RGS7 in heart confirming that RGS7 increases acetylation of SIRT1 substrates and thereby drives cardiac dysfunction. Together, our data identify RGS7 as an amplifier of inflammatory signaling in heart and possible therapeutic target in chemotherapeutic drug-induced cardiotoxicity.

Keywords RGS proteins · Acetylation · Chemotherapy · Cardiotoxicity · Inflammation · Fibrosis

Introduction

The anthracycline chemotherapeutic doxorubicin has been in clinical use since 1974 and remains among the most versatile and widely used drugs in the treatment of solid tumors and hematological malignancies. However, the clinical utility

Madhuri Basak and Kiran Das have equally contributed this work.

✉ Adele Stewart
stewarta@health.fau.edu

✉ Biswanath Maity
bmaity28@gmail.com; bmaity@cbmr.res.in

[1] Centre of Biomedical Research (CBMR), SGPGI, SGPGI Campus, Raebareli Road, Lucknow, Uttar Pradesh 226014, India

[2] Department of Biosciences and Bioengineering, Indian Institute of Technology Roorkee, Roorkee, Uttarakhand 247667, India

[3] Institute of Pharmaceutical Sciences, University of Lucknow, Lucknow, Uttar Pradesh 226025, India

[4] Department of Chemistry, SRM Institute of Science and Technology, Kattankulathur, Chennai, Tamilnadu 603203, India

[5] Department of Biomedical Science, Charles E. Schmidt College of Medicine, Florida Atlantic University, Jupiter, FL 33458, USA

of doxorubicin is constrained by dose-limiting and occasionally life-threatening cardiotoxicity. Patients undergoing treatment with doxorubicin are at high risk of developing left-ventricular dysfunction that may remain asymptomatic or progress into congestive heart failure. At a cumulative doxorubicin dose of 400 mg/m^2, the incidence of heart failure is 5%, though it increases to 48% at a dose of 700 mg/m^2 and 65% if subclinical cardiac events are included [1]. The time course of disease presentation is highly variable and the onset of detectable loss of ventricular function may occur months or even years following drug exposure, an observation that has proven particularly problematic for childhood cancer survivors [2]. The drug dexrazoxane, which competes with doxorubicin for topoisomerase 2β binding [3], does minimize cardiac damage but also compromises the tumoricidal properties of anthracyclines [4]. Thus, strategies aimed at mitigation of doxorubicin cardiotoxicity are confined to first-line heart failure medications such as ACE inhibitors and β blockers [5] that have been shown to normalize left-ventricular ejection fraction (LVEF) in only 42% of patients [6] underscoring the need for more efficacious interventions and improved prognostic biomarkers.

The etiology of chemotherapeutic cardiomyopathy remains poorly understood, but several key processes have been implicated. Because of their high metabolic demand and mitochondrial volume, cardiomyocytes are particularly susceptible to oxidant damage [7] and doxorubicin triggers rapid oxidative stress and cell death by compromising mitochondrial function, actions known to involve inhibition of topoisomerase 2β [8] as well as generation of reactive oxygen species (ROS) via several DNA-damage independent mechanisms [9–12]. While loss of viable myocytes immediately following doxorubicin exposure undoubtedly compromises cardiac contractility, the maladaptive fibrotic remodeling and inflammation triggered following repeated drug administration further exacerbates heart damage. Deficiency in several Toll-like receptors (TLRs) prevents doxorubicin-dependent oxidative stress, cell death, fibrosis, and inflammation, and improves cardiac function and survival [13–16]. These receptors play a key role in sensing cellular detritus released from apoptotic cells and facilitate further immunogenic cell death by promoting activation of nuclear factor kappa-light-chain-enhancer of activated B cells (NF-κB) and production of tumor necrosis factor α (TNFα) [17, 18]. TNFα receptor signaling is required for doxorubicin-dependent neutrophil recruitment [19], and depletion of neutrophils [20] or maintenance of reparative macrophages [21] protects against the damaging impacts of doxorubicin in the heart. A complex milieu of pro-apoptotic and pro-fibrotic cytokines are also released from transdifferentiated myofibroblasts and infiltrating neutrophils and macrophages contributing to sustained, high-grade sterile inflammation [22]. Though critical for doxorubicin-induced cardiomyopathy, targeting the innate immune system per se might increase tumor burden. Thus, a more selective means to circumvent or prevent inflammation specifically in the myocardium is required.

Depletion of Regulator of G-protein signaling 7 (RGS7) in the myocardium improves left-ventricular function following chronic doxorubicin administration [23]. Prior work demonstrated that RGS7 functions in myocytes to promote mitochondrial dysfunction, Ca^{2+} overload, and cell death, but RGS7 overexpression in heart also drives release of cytokines neuregulin 1 (NRG1) and transforming growth factor β1 (TGFβ1) [23]. In liver, RGS7 promotes accumulation of TNFα in response to lipotoxic stress, an action required for the ability of RGS7 to promote hepatic inflammation, fibrosis, oxidative stress, and cell death [24]. TNFα has also been shown to increase RGS7 phosphorylation, thereby preventing proteasomal degradation of RGS7 in brain [25, 26], suggesting that RGS7 accumulation may act in a feed-forward manner to amplify cytokine action. It remains unclear, however, if the pro-inflammatory actions of RGS7 are secondary to cell loss or a direct impact of RGS7 on signaling cascades of the innate immune system. RGS proteins canonically function to control signaling via G-protein-coupled receptors on the cell surface. However, RGS7 has been shown to shuttle between the plasma membrane and nucleus[27] and binds to nuclear proteins, such as activating transcription factor 3 (ATF3) and histone acetyltransferase KAT5 (Tip60)[24]. Among the key targets of Tip60 is the NF-κB family member p65 (RelA), a pivotal transcriptional mediator of the inflammatory response. Tip60 binds to p65 and promotes NF-κB acetylation [28], a reversible modification required for full NF-κB transcriptional activity [29]. The NAD-dependent deacetylase sirtuin 1 (SIRT1), which suppresses doxorubicin-dependent cardiotoxicity by decreasing myocyte apoptosis and induction of inflammatory mediators[30–32], antagonizes NF-κB activity by deacetylating the Tip60-sensitive Lys 310 residue on p65[33]. However, whether SIRT1-dependent p65 de-acetylation is involved in the ability of SIRT1 to suppress doxorubicin-driven heart damage has yet to be established.

We hypothesized that RGS7 may directly activate NF-κB by facilitating Tip60-driven NF-κB acetylation and/or suppressing the actions of SIRT1. Here, we describe a critical role for RGS7 in doxorubicin-dependent cardiac inflammation and fibrosis, actions that involve differential complex formation between RGS7 and Tip60 or SIRT1.

Materials and methods

Materials

The source/catalog information for all reagents (Table S1), antibodies (Table S2), assay kits (Table S3), and cell lines (Table S4) can be found in Supplementary Tables 1–4.

Animals

Male Swiss albino mice (25–30 g) were reared on a balanced laboratory diet [Nutrimix STD – 1020; Nutrivet Life Sciences, Pune, Maharashtra, India] as per NIN, Hyderabad, India and given tap water and food ad libitum. Male mice were used due to their enhanced susceptibility to doxorubicin-induced cardiotoxicity [34]. They were kept at 20 ± 2 °C, 65–70% humidity, and day/night cycle (12 h/12 h).

In vivo *RGS7 knockdown (KD) and doxorubicin treatment*

To achieve cardiac knockdown of RGS7 1-week-old wild-type (WT) mice received a single intraventricular injection of 4.5 X 10^8 lentiviral vectors containing scramble or RGS7-targeted small hairpin RNA (shRNA; Santa Cruz Biotechnology, Dallas, TX, USA) in a 40 µl volume and packaged for delivery with Invivofectamine 3.0 (ThermoFisher Scientific). Lentiviral particles were generated in AC-16 cells as per a standard protocol. After injection, mice were returned to their mothers until weaning and allowed to age to adulthood (8–10 weeks) for subsequent experiments. For chronic chemotherapy treatment, mice received multiple doses of doxorubicin (cumulative dose of 45 mg/kg i.p.; 9 mg/kg every other week) or saline over a period of 10 weeks ($n = 10$/group). 1 week after the final drug dose mice were euthanized by cervical dislocation and blood/tissues were collected for downstream analysis. The dose of doxorubicin used for chronic administration was calculated from a typical doxorubicin treatment schedule (40–75 mg/m^2 intravenously every 21 days) by adjusting for the relative body surface area of a human versus mouse [35]. To correct the bioavailability of doxorubicin when administered via intraperitoneal injection versus intravenously (~44%) [36], we altered the schedule to biweekly administration. RGS7 knockdown was verified via immunoblotting. Following intra-cardiac injection, body weight (1X/week) and food intake (1–2X/week) were monitored. No notable alterations in animal weight, food intake, or general well-being were found.

Cardiac RGS7 overexpression and resveratrol treatment

Generation of constructs for viral RGS7 overexpression has been previously described [23]. Lentiviral particles were generated in AC-16 cells as per a standard protocol. For RGS7 overexpression, 70 µL of lentivirus containing 2×10^8 particles of either mRGS7-Lenti or a control empty vector virus were packaged for delivery with Lipofectamine 2000 (Thermo Fisher Scientific) and administered via intra-cardiac injection when WT mice were 9–10 weeks old. Following RGS7 overexpression, the animal cohort was divided with half receiving saline and half resveratrol (20 mg/kg, i. p., 2 times per week, 3 weeks) beginning 15 days after viral injection ($n = 10$/group). Resveratrol dose was chosen based on prior studies investigating the protective actions of the drug in doxorubicin-induced cardiotoxicity [37–39]. Animals were sacrificed 3 days after the final resveratrol injection and tissues were isolated for downstream analyses.

Cardiac phenotyping

We used two-dimensional echocardiography to determine cardiac function in vivo. Using an ultrasound system (Vivid S5 system, GE Healthcare, USA), we measured the left-ventricular parameters (left-ventricular end-diastolic and systolic pressure; LVEDP and LVESP) and LVEF on lightly sedated mice treated with chemotherapeutic drugs and/or RGS7KD as described earlier.

Histology and immunohistochemistry

Paraffin-embedded formalin-fixed mouse and human heart tissue sections were stained with Masson trichome (Sigma, St. Louis, MO) to detect tissue collagen deposition. Regents were utilized as per the manufacturer's protocols. The blue-stained collagen in tissue section image stained with Masson trichrome was processed using the "Threshold" tool of Image J software (NIH, USA) and the fraction of the total area that was stained blue was quantified. Immunohistochemical staining of both mouse and human tissue sections was performed as per a standard protocol [40]. For RGS7, Ac-p65, Tip60, and SIRT1 staining, 7–10 sections were stained from each animal with 5 pictures randomly selected from each slide for quantification using Image J.

Immunoblotting

Tissues were rapidly dissected from mice and flash-frozen in liquid nitrogen. Tissue homogenates and cell lysates were prepared in RIPA buffer containing protease and phosphatase inhibitors (Sigma), quantified, and probed as previously described [40]. Twenty µg of protein per sample was

subjected to SDS-PAGE and immunoblotting using standard techniques. Immunoblots were developed using the chemiluminescence method with HRP-labeled secondary antibodies. Antibody dilution and catalog information can be found in Table S2. Densitometric quantification of western blots was performed utilizing Image J software (NIH). Protein expression was normalized to loading control (β-Actin) and expressed relative to control conditions.

Cell isolation and culture

Primary ventricular cardiomyocytes (VCM) and fibroblasts (VCF) were isolated from 8 to 10-week-old adult mice according to a published protocol [41]. The human cardiomyocyte cell line AC-16 (Merck, Darmstadt, Germany) was cultured in DMEM and 10% FBS (Gibco, Waltham, MA, USA) in a 37 °C incubator at 5% CO_2 with 10% FBS. Cells were transduced with lentiviral vectors encoding shRGS7 or control shRNA (Santa Cruz Biotechnology) according to the manufacturer's instructions. Cells were transduced with constructs encoding the full-length RGS7 protein or mutants lacking the Gγ-like (GGL)/RGS, Disheveled, Egl-10 and Pleckstrin homology (DEP), GGL only, or RGS domains (Δ251-469, Δ1-136, Δ256-315, and Δ327-446, respectively). Drug treatments were initiated 16 h after construct introduction.

Drug treatment of cultured cells

Cells were treated with doxorubicin (3 μM, 16 h) in the presence or absence of pre-treatment with resveratrol (20 μM, 4 h), the Tip60 inhibitor NU9056 (5 μM, 3 h), or the TNFα inhibitor adalimumab (7 μg/ml, 1 h) where indicated. The doxorubicin dose used in cultured cells was chosen based on prior reports investigating the toxic actions of doxorubicin in human cardiomyocytes [23, 42, 43]. Drug concentrations were chosen based on levels sufficient to block doxorubicin-dependent cellular signaling in prior reports or sufficient to activate/block the target protein [44–47]. In a separate experiment, co-cultured murine VCM and VCF were treated with control serum, serum from patients with a history of chemotherapy but without cardiac fibrosis, or 10% serum from patients with cardiac fibrosis for 12 h. For conditioned media experiments, cells were initially cultured in standard culture media until cells were 80–85% confluent. The media was then replaced with serum-free DMEM, and drugs were added. After replacing the media again and rinsing the cells, cells were incubated for an additional 16 h in drug/serum-free media. This "conditioned media" (CM) was collected from donor cells and then used to replace standard media on recipient cells. Recipient cells were collected for further processing after 16 h.

Immunoprecipitation

AC-16 cells (3×10^6) were lysed, and protein concentration was measured via BCA protein assay. 600 μg of protein was equilibrated in IP lysis buffer (50 mM Tris, 5 mM EDTA, 250 mM NaCl, and 0.1% Triton X-100) and pre-cleared with 30 μl of Protein G Sepharose beads (Abcam, Cambridge, UK). Next, bait antibodies (GFP, RGS7, Tip60, SIRT1, or control mouse IgG) were added and samples incubated for 12 h on a rotor at 4 °C. 30 μl of Protein G Sepharose beads (Abcam) were equilibrated in IP buffer and then added to lysate. After a 2-h incubation, bead slurries were centrifuged and washed 3X with IP buffer. Immunocomplexes were eluted in non-reducing laemmli buffer at 95 °C and subjected to SDS-PAGE and immunoblotting with prey antibody (Tip60, SIRT1, or RGS7).

Measurement of ROS generation

ROS generation was estimated in tissue and primary cell lysates using the cell-permeable oxidation-sensitive probe, CM-H_2DCFDA (2′,7′-dichlorodihydrofluorescein diacetate) as described previously [48]. Cells were harvested by centrifugation, washed three times with ice-cold phosphate buffered saline (PBS), re-suspended in PBS, and incubated with 5 μM CM-H_2DCFDA (Sigma) for 20 min at 37 °C. After incubation cells were again washed and lysed in PBS with 1% Tween 20. Tissue lysates were prepared in a standard RIPA buffer. ROS level was determined at the ratio of dichlorofluorescein excitation at 480 nm to emission at 530 nm. The CM-H_2DCFDA assay is utilized as a general oxidative stress indicator and not as a detector of a specific oxidant due to known limitations of the probe [49].

ELISAs and enzymatic assays

A summary of commercially available kits used to measure cell death (apoptosis; cytoplasmic histone-associated DNA fragments), NF-kB activity, and MMP-9 activity is available in Table S3. Cells/tissues/samples were harvested, and samples were processed according to the manufacturer's instructions.

Cell viability

The MTT reduction assay was used to monitor cell viability. 5×10^4 cells/well were seeded in 48-well plates with DMEM + 10% FCS. The MTT (Sigma) solution was

prepared at 1 mg/mL concentration in medium without phenol red, and 200 µL of MTT solution was added to each well. The cells were incubated for 2 h at 37 °C. 200 µL of DMSO was then added into each well for solubilization of the formed formazan crystals. The optical density of the wells was determined at a wavelength of 550 nm (Biotek Instruments).

YASARA homology modeling of RGS7 & in-silico molecular docking and molecular dynamics (MD) simulations

The amino-acid sequence of RGS7 was used as an input (in FASTA format) and the default homology modeling macro of YASARA structure was executed to generate the structural model of RGS7. First, the binary complex between homodimeric RGS7 and KAT5 was generated using the ZDOCK web server application (https://zdock.umassmed.edu) [50]. Next, the SIRT1 structure was docked on binary RGS7-KAT5 complex again using the ZDOCK server. RGS7/KAT5 (Tip60) binary and ternary structures were simulated for 200 ns using GROMACS 2020.5. The gromacs structure was prepared using gmx pdb2gmx module, and topologies were defined using Charmm36 force field and TIP3P water model. The protein was solvated in a 1.0 nm cubic box and neutralized with chloride ions. Energy minimization was performed using the steepest descent algorithm for 5000 steps until the maximum force reaches < 1000 kJ/mol/nm to remove any steric clashes in the system. Equilibration phase was further carried out for 5 ns at pH 7, respectively. During both NVT and NPT ensembles, the system temperature was maintained at 300 K using Berendsen's weak coupling method. The pressure was maintained at 1 bar using the Parrinello–Rahman barostat during the NPT ensemble. The final MD production was carried out for 200 ns using a time step of 2 fs and the LINCS algorithm. For trajectory analysis, root-mean-square deviations (RMSD), radius of gyration (Rg), chain-wise root-mean-square fluctuations (RMSF), Solvent accessible surface area (SASA), and Hydrogen bonding between protein and solvent were analyzed. For the analysis of amino-acid residues present on protein-protein interaction interface, the SASA calculations were performed using the InterProSurf Webserver (http://curie.utmb.edu/usercomplex.html) [51]. The analysis involves the SASA calculation of residues in the complex and in the isolated subunits; the residues showing significant change in the SASA value were considered most likely to be on the interaction interface.

Study approval

Mouse experiments were performed at the Aryakul College of Pharmacy & Research, Lucknow, India. Animals were procured after obtaining clearance from the college Animal Ethics Committee (1896/PO/Re/S/16/CPCSEA/2021/5) and were handled following International Animal Ethics Committee Guidelines and in agreement with the Guide for the Use and Care of Laboratory Animals (NIH). Post-mortem human tissue samples and serum samples were acquired from the Department of Forensic Medicine, Sagore Dutta Medical College & Hospital, Kolkata, West Bengal after obtaining the ethical clearance from the Centre of Biomedical Research Ethics Committee (Ref: IEC/CBMR/Corr/2020/16/6). For the 'no fibrosis' group, serum was taken after a minimum of 8 months of chemotherapy treatment after verification that no clinical fibrosis symptoms were present. For the 'fibrosis' group, serum was taken after endocardial biopsy (EMB) confirmed the presence of fibrosis after chemotherapy treatment. The presence of myocardial fibrosis was confirmed by either the presence of a fragmented QRS complex on electrocardiogram (ECG) or by measuring fractional collagen volume. Information on the sex, age, cause of death, co-morbid conditions, and chemotherapy history for all heart autopsy samples is available in Table S5. To stratify patient samples based on cardiac health, tissues from patients with a history of chemotherapy were stained with Masson Trichrome (as above) to detect fibrotic remodeling. In collaboration with a pathologist, sections were scored on the following scale: 0–1, no fibrosis or a very small ischemic scar; 2, moderate sized ischemic scar; 3, moderate ischemic scar and collagen deposition in the extracellular space; 4, widespread collagen deposition. Samples with scores ≤ 1 were categorized as "chemotherapy -fibrosis" and samples with scores ≥ 2 were categorized as "chemotherapy + fibrosis". Patients classified as "heart failure" patients had an LVEF < 40, the newly accepted universal cutoff for heart failure with reduced EF [52]. We should also note that we do not have complete dosing/schedule information for anticancer regimens or additional pharmacological interventions for co-morbid conditions used for each patient, and this is a limitation of our analysis of post-mortem human cardiac tissue.

Results

RGS7 up-regulation is associated with inflammation in the hearts of patients with a history of chemotherapy

In our prior report, we demonstrated that chemotherapy exposure is associated with RGS7 up-regulation in the heart [23]. Paralleling alterations in RGS7 expression and induction of fibrosis and heart failure markers, such as atrial natriuretic peptide (ANP), β myosin heavy chain (β-MHC),

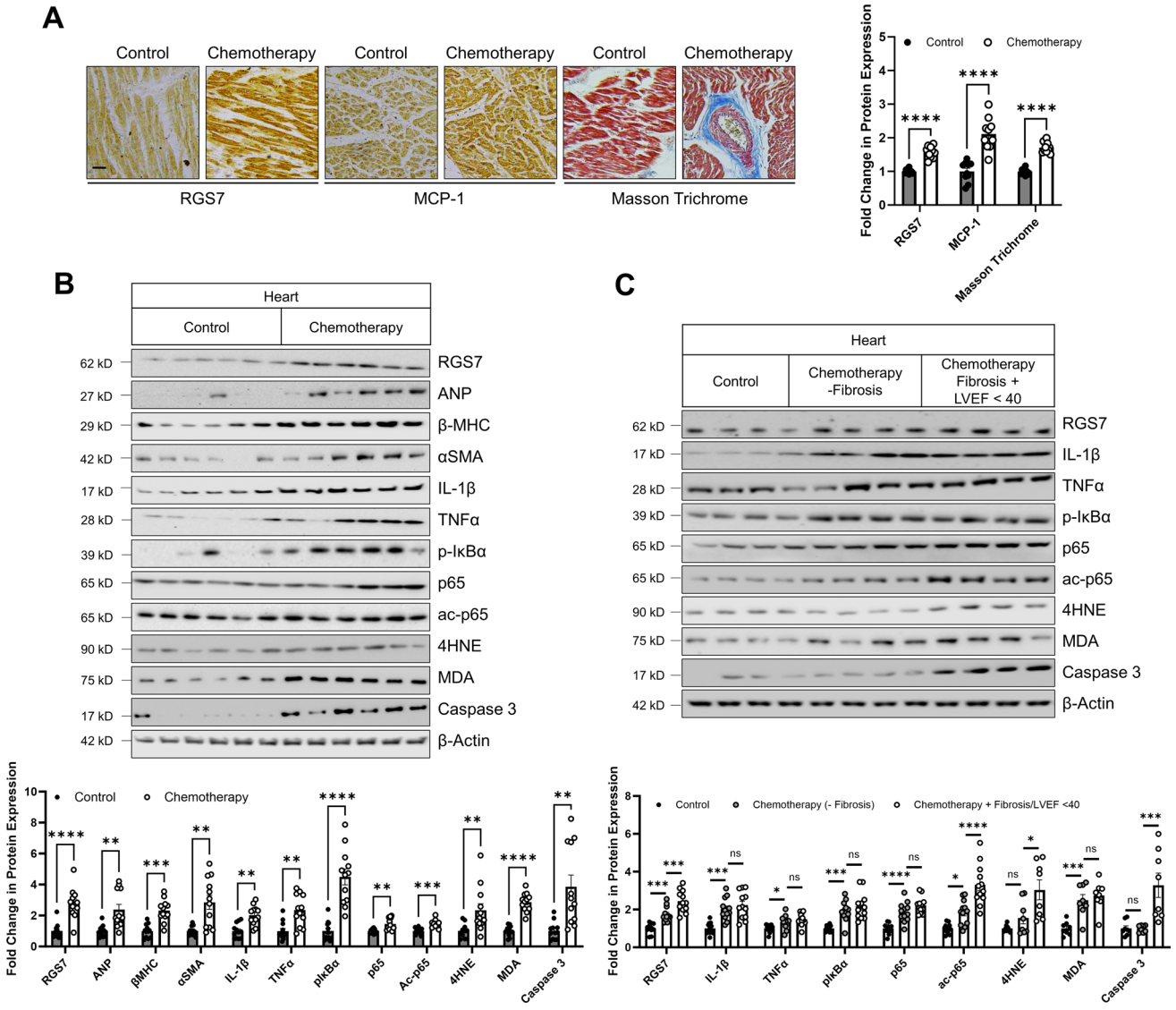

Fig. 1 RGS7 up-regulation is accompanied by increases in inflammatory mediators in the hearts of patients with a history of chemotherapy. **A** Representative staining and quantification of cardiac RGS7, MCP-1, and Masson trichrome levels in control (black circles, $n = 10$) or patients with a history of chemotherapy (white circles, $n = 10$) [scale bar = 100 μm]. **B** Representative immunoblots and quantification of RGS7, ANP, β-MHC, αSMA, IL-1β, TNFα, p-IκBα, p65, ac-p65, 4HNE, MDA, and cleaved caspase 3 expression in heart tissue lysates from patients with a history of chemotherapy and controls ($n = 10$/group). **C** Representative immunoblots and quantification of cardiac RGS7, IL-1β, TNFα, p-IκBα, p65, ac-p65, 4HNE, MDA, and cleaved caspase 3 expression in controls and patients with a history of chemotherapy stratified based on cardiac function (no heart failure or heart failure; $n = 8$–10/group). A detailed history of chemotherapy patients and controls is provided in Table S5. β-Actin serves as a loading control for immunoblots. Data were analyzed by Student's *t* test or one-way ANOVA with Sidak's post hoc test. $^{*}P < 0.05$, $^{**}P < 0.01$, $^{***}P < 0.001$, $^{****}P < 0.0001$. *ns* not significant. Data are presented as mean ± SEM

and α smooth muscle actin (αSMA), and human patients with a history of chemotherapy, display increased levels of monocyte chemoattractant protein-1 (MCP-1), interleukin 1β (IL-1β), TNFα, and NF-κB cascade components p65, acetylated p65, and phosphorylated IκBα indicative of ongoing inflammation (Fig. 1A, B). We also noted an increase in indicators of oxidative stress, such as the lipid peroxidation markers 4-hydroxynonenal (4HNE) and malondialdehyde (MDA) (Fig. 1B). An increase in RGS7 expression was also found in human cardiac tissue following myocardial infarction implicating RGS7 as a universal indicator of cardiac damage (Fig. S1A). Notably, while IL-1β, TNFα, p-IκBα, total p65, and MDA expression were elevated in patients with a history of chemotherapy and detectable fibrosis but no evidence of congestive heart failure, we noted that RGS7, p65 acetylation, and apoptosis executioner caspase 3

induction were further exacerbated in individuals with heart failure (Fig. 1C). As we cannot control for the influence of variables such as co-morbid pathological conditions, specific cause of death, and additional pharmacological interventions in the history of each patient, this prompted us to explore a possible causative role for RGS7 in cardiac inflammation in a controlled manner using a combination of in vitro human and murine cells as well as in vivo in mice.

Cardiac RGS7 knockdown ameliorates doxorubicin-dependent inflammation in heart

When co-cultured murine VCF and VCM were exposed to serum isolated from patients with a history of

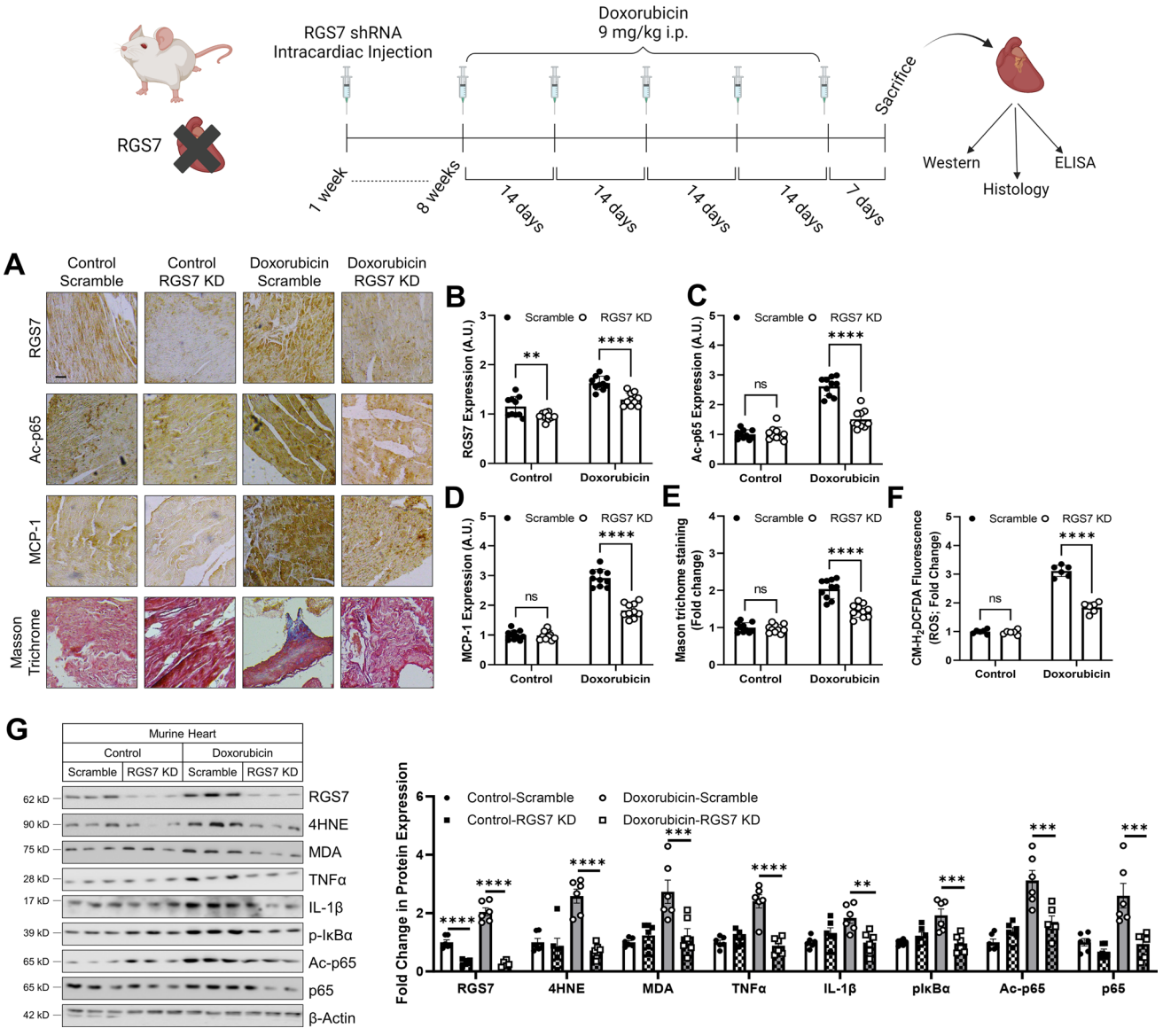

Fig. 2 Cardiac-specific RGS7 knockdown ameliorates chemotherapy-dependent inflammation and fibrosis in mice. **A–G** Following administration of scramble or RGS7-shRNA via intra-cardiac injection (P7), mice were treated with doxorubicin (9 mg/kg, i.p. biweekly; cumulative dose of 45 mg/kg) or saline beginning when mice were 9 weeks of age. Samples were collected 1 week after the last dose later for biochemical and histological analyses. **A** Representative immunostaining for RGS7, acetylated p65 (Ac-p65), and MCP-1 and Masson Trichrome staining in heart tissue sections [scale bar = 100 µm]. Quantification of **B** RGS7, **C** Ac-p65, **D** MCP-1, and **E** Masson trichrome was performed ($n = 10$). **F** CM-H_2DCFDA fluorescence in cardiac lysates (ROS; $n = 6$). **G** Representative immunoblots and quantification of cardiac RGS7, 4HNE, MDA, IL-1β, TNFα, p-IκBα, p65, and ac-p65 expression ($n = 6$). β-Actin serves as a loading control for immunoblots. Diagram was created using Biorender.com. Data were analyzed by two-way ANOVA with Sidak's post hoc test. $^{**}P < 0.01$, $^{***}P < 0.001$, $^{****}P < 0.0001$. *ns* not significant. Data are presented as mean ± SEM

chemotherapy with detectable cardiac fibrosis, RGS7 levels increased, indicating that a secreted factor, present in the circulation of individuals with a history of chemotherapy, drives RGS7 induction in cardiac cell types (Fig. S1B). These data beg the question as to whether RGS7, previously implicated in chemotherapy-dependent myocyte apoptosis [23], drives inflammation or is simply a secondary consequence of ongoing pro-fibrotic and inflammatory cytokine release. To test this hypothesis, we utilized RGS7-targeted shRNA delivered directly to the heart via intra-cardiac injection to deplete RGS7 levels in the myocardium prior to doxorubicin treatment. As expected, chronic, low-dose doxorubicin exposure triggered RGS7 up-regulation (Fig. 2A, B), acetylation-dependent p65 activation (Fig. 2A, C, G), MCP-1 accumulation (Fig. 2A, D), collagen deposition (Fig. 2A, E), ROS generation (Fig. 2F), lipid peroxidation (Fig. 2G; 4HNE, MDA), and inflammatory cytokine induction (Fig. 2G; TNFα, IL-1β) in the heart. Importantly, all these endpoints were improved by 50% or more in doxorubicin-treated mice following RGS7 knockdown in the heart (Fig. 2A–G).

RGS7 forms a complex with Tip60 and SIRT1 in myocytes and modulates their expression

Having identified RGS7 as a key driver of doxorubicin-dependent cardiac inflammation, we next sought to identify the mechanism by which RGS7 influences immune system activation in heart. RGS proteins canonically function to control signaling via G-protein-coupled receptors (GPCRs). However, RGS7 subserves several GPCR-independent functions in non-neuronal cell types having been identified as a binding partner for the acetyltransferase Tip60, actions required for the ability of RGS7 to promote lipotoxic stress and inflammation in liver via a mechanism requiring TNFα production [24]. How the RGS7/Tip60 complex drives inflammatory cytokine production remains unknown. Given the close correlation between RGS7 and p65 acetylation in human heart, we hypothesized that RGS7 might promote inflammation by controlling acetylation of p65 by Tip60. Indeed, Tip60 expression is increased following chemotherapy exposure in the human heart as assessed by either immunohistochemistry (Fig. 3A) or immunoblot (Fig. S2). Notably, a diametrically opposed trend was observed for the deacetylase SIRT1 (Fig. 3A, S2) indicating a likely shift in acetylation probability. In fact, we found that RGS7 can be co-immunoprecipitated with both Tip60 and SIRT1 and that doxorubicin treatment shifts the relative abundance of RGS7 complexes from those containing SIRT1 to those containing Tip60 (Fig. 3B). Mapping of the Tip60/SIRT1-binding interface on the RGS7 protein revealed that elimination of either the DEP or RGS domains impaired complex formation with both Tip60 and SIRT1, indicating that they may bind to the same portion of the RGS7 protein (Fig. 3C).

To gain structural insights into the protein-protein interactions between RGS7 and Tip60/SIRT1, we performed an MD simulation of the binary (RGS7/Tip60) and ternary (RGS7/Tip60/SIRT1) complexes. 3D structures of the highest binding energy for the binary (RGS7-Tip60) and ternary (RGS7–Tip60–SIRT1) complexes (Fig. 3D) were used to perform the MD simulation. The RMSD plots revealed that both binary and ternary complexes are exquisitely stable in solution as reflected by the virtually invariant RMSD values over the simulation, a metric that reflects the average distance between atoms in each protein (Fig. 3E). However, the average RMSD for the ternary complex was found to be less than that of binary complex indicative of a more compact and stable ternary structure. The Rg of the RGS7–Tip60–SIRT1 complex was also more stable across the simulation (Fig. 3F) and lacked the decrease in Rg observed after 100 ns with RGS7–Tip60 alone, which may represent a structural transition of the complex toward a more compact globular state. The improved structural stability of the RGS7–Tip60–SIRT1 complex over the RGS7–Tip60 complex alone was further confirmed by the time stability of SASA values (Fig. S3A) and the number of H-bonds (Fig. S3B), which lacked major fluctuations likely because all monomers present in the complexes are tightly bound to each other and the quaternary structure of the complexes is preserved and stable over the course of simulation time. Similarly, the RMSFs were lower for the ternary vs binary complex (Fig. S4). When SASA calculations were performed to identify the amino acids present at the protein-protein interaction interfaces, several RGS7 residues were identified that underwent a significant change all of which lay within the RGS domain (aa 324–450; Table S6). Consistent with a role for RGS7 in controlling Tip60/SIRT1 action, cardiac RGS7 knockdown decreased Tip60 expression and increased expression of SIRT1 following doxorubicin exposure when measured via either immunohistochemistry (Fig. 3G) or immunoblot (Fig. 3H).

RGS7 regulates the abundance of Tip60 and SIRT1 and activation of inflammatory signaling in cardiac myocytes

We recapitulated the molecular signature observed in human and murine tissue in a culture system, showing that, as observed in vivo, doxorubicin treatment increased protein expression of RGS7 and Tip60, decreased SIRT1, and increased inflammatory markers, such as IL-1β, TNFα, p65, phospho-IκBα, and acetylated p65 in both murine VCM (Fig. S5A) and the human cardiomyocyte cell line AC-16 (Fig. S5B). Importantly, RGS7 knockdown in either AC-16 cells (Fig. 4A) or murine VCM (Fig. S6A) completely prevented these changes, indicating that the ability of RGS7 to

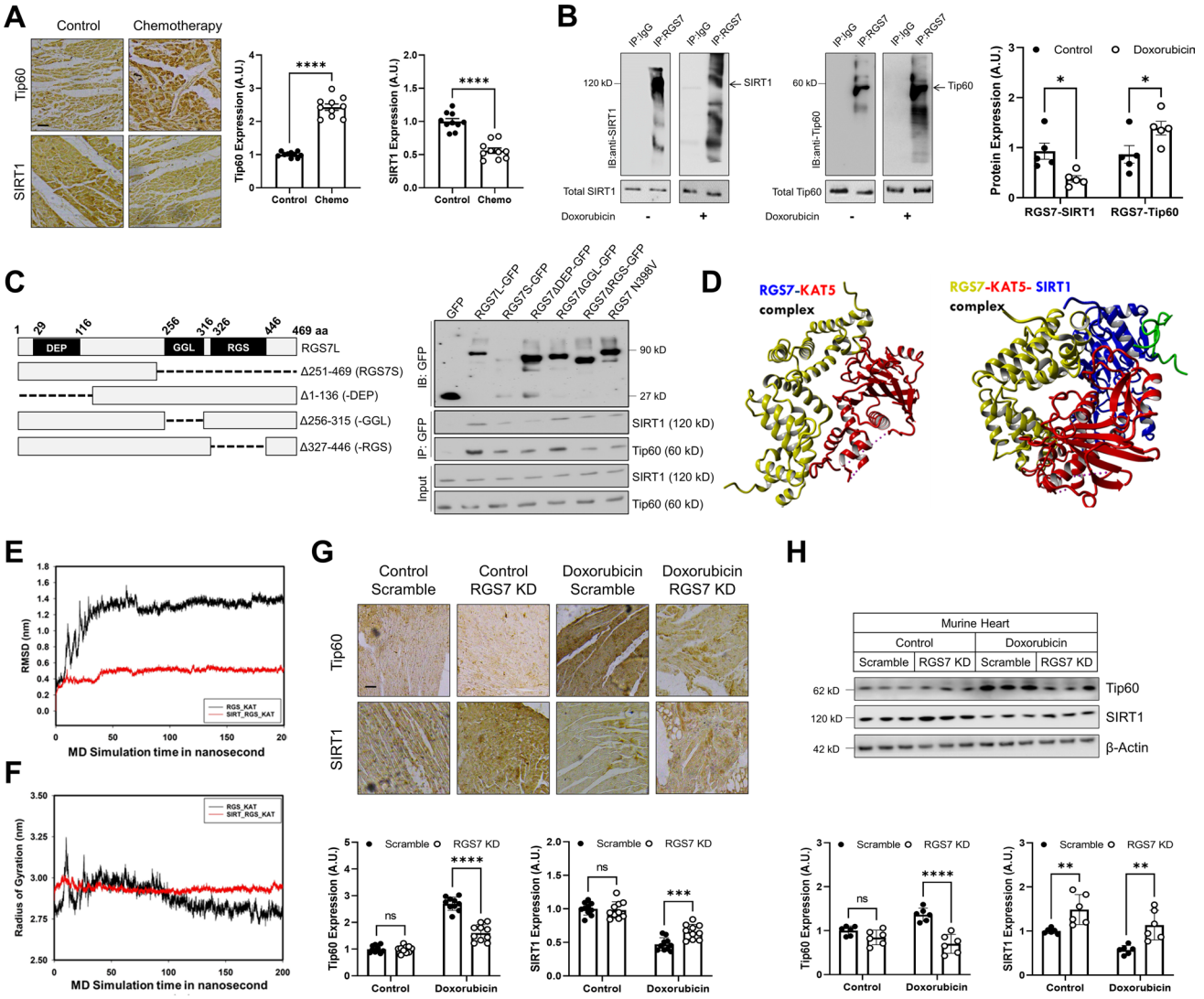

Fig. 3 RGS7 forms a complex with SIRT1 and Tip60 in VCM. **A** Representative staining and quantification of cardiac Tip60 and SIRT1 expression in control ($n=10$) or patients with a history of chemotherapy ($n=10$) [scale bar = 100 µm]. **B** Co-IP of RGS7 with SIRT1 or Tip60 from human AC-16 cardiomyocytes ± doxorubicin (3 µM, 16 h). Data were quantified from five independent experiments (right panel). **C** Co-IP SIRT1 and Tip60 with RGS7 deletion constructs from human AC-16 cardiomyocytes. **D** In silico modeling of RGS7–Tip60–SIRT1 complex support a direct RGS7 interaction. Tip60 protein (Lys178-Pro452) on the surface of RGS7 (homodimeric form, Ser318-Ala458) (left) and SIRT1 (Sirtuin-1) on the surface of binary RGS7–Tip60 complex (right). Plot showing **E** RMSD and **F** Radius of gyration (Rg) values for the binary RGS7—Tip60 (in black) and ternary RGS7–Tip60–SIRT1 (in red) complexes evaluated as a function of simulation time. Representative images and quantification of **G** immunohistochemical staining ($n=10$) [scale bar = 100 µm] and **H** immunoblotting ($n=6$) for cardiac Tip60 and SIRT1 in mice (± doxorubicin, ± RGS7 shRNA) treated as in Fig. 2. β-Actin serves as a loading control for immunoblots. Data were analyzed by Student's *t* test or two-way ANOVA with Sidak's post hoc test. $^{*}P<0.05$, $^{**}P<0.01$, $^{***}P<0.001$, $^{****}P<0.0001$. *ns* not significant. Data are presented as mean ± SEM

promote inflammation following doxorubicin exposure is, at least in part, due to myocyte-intrinsic mechanisms. We also found that myocytes in which RGS7 had been depleted were resistant to doxorubicin-induced ROS generation (Fig. 4B, S6B), NF-κB activation (Fig. 4C, S6C), and cell death (Fig. 4D, S6D).

Tip60 activation and SIRT1 inhibition are required for RGS7-dependent inflammatory signaling in myocytes

In AC-16 cells, RGS7 overexpression phenocopied several key impacts of doxorubicin treatment, including increased p65 acetylation, production of TNFα and IL-1β, and increased expression of lipid peroxidation marker 4HNE

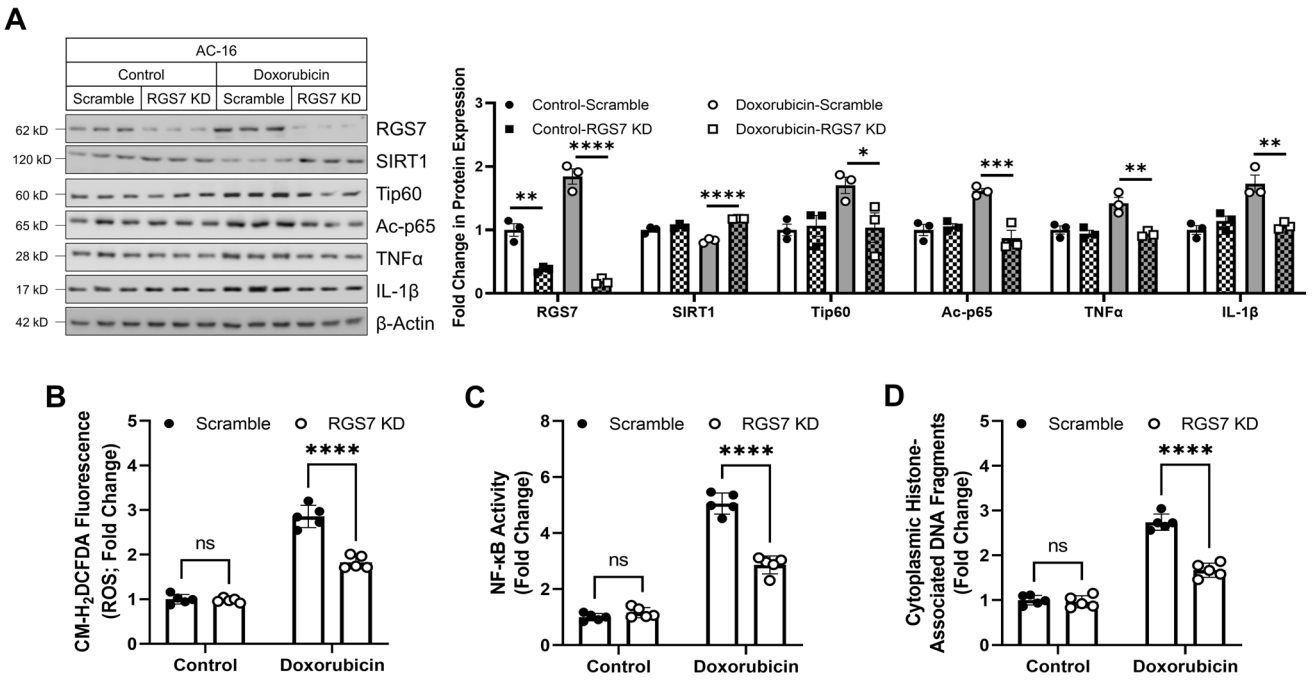

Fig. 4 RGS7 knockdown protects against doxorubicin-induced inflammatory cytokine production in human AC-16 cardiomyocytes. AC-16 cells were treated with doxorubicin (3 μM, 24 h) 24 h following administration of scramble or RGS7-specific shRNA. **A** Immunoblotting for RGS7, SIRT1, Tip60, p65 acetylation, TNFα, and IL-1β with quantification ($n=3$). **B** CM-H_2DCFDA fluorescence (ROS; $n=5$). **C** NF-kB activity ($n=5$). **D** Apoptosis (cytoplasmic histone-associated DNA fragments; $n=5$). Data were analyzed by two-way ANOVA with Sidak's post hoc test. *$P<0.05$, **$P<0.01$, ***$P<0.001$, ****$P<0.0001$. *ns* not significant. Data are presented as mean ± SEM

(Fig. 5A) as well as increased ROS generation (Fig. 5B), activation of NF-κB (Fig. 5C), and cell death (Fig. 5D). To test if the pro-inflammatory, pro-oxidant, and pro-apoptotic actions of RGS7 could be attributed to differential protein acetylation, we treated AC-16 cells with either the Tip60 inhibitor NU9056 or sirtuin activator resveratrol. As anticipated, either Tip60 inhibition (Fig. 5A–D) or sirtuin activation (Fig. 5E–H) decreased p65 acetylation, NF-κB activation, ROS generation, and cell death by 50% or more following RGS7 overexpression. Nearly identical results were obtained in murine VCM (Fig. S7A–F), emphasizing that the mechanism(s) driving RGS7-dependent inflammatory cytokine production and trigger cell death are conserved across species. Together, these data indicate that the ability of RGS7 to drive inflammation requires Tip60 activation and/or SIRT1 suppression.

RGS7-dependent release of pro-fibrotic and pro-inflammatory factors from myocytes drives fibrosis

We hypothesized that RGS7-dependent release of pro-fibrotic and inflammatory cytokines from damaged and dying myocytes might play a key role in promoting VCF transdifferentiation and fibrotic remodeling in the myocardium following a cardiotoxic insult. To test this idea in a controlled manner, we first exposed VCM transduced with scramble or RGS7-targeted shRNA to doxorubicin, removed the drug, and collected the media from the damaged cells. Presumably, any cytokines produced by these myocytes in response to doxorubicin treatment would be excreted into the media and could then be collected and used to activate fibroblast cultures. Indeed, exposure of VCF to this conditioned media was sufficient to increase oxidative stress (Fig. 6A), compromise cell viability (Fig. 6B), and induce activation of the matrix remodeling protein matrix metalloproteinase 9 (MMP-9) (Fig. 6C). We also noted that markers of fibroblast transdifferentiation (αSMA) and fibrosis (collagen 1α; Col1α) as well as inflammatory mediators phospho-IκBα, p65, TNFα, and IL-1β were increased in VCF following exposure to conditioned media from doxorubicin-treated VCM (Fig. 6D). Consistent with a loss of cytokine production from VCM following RGS7 depletion, introduction of RGS7 shRNA to VCM was sufficient to mitigate these impacts (Fig. 6A–D). We observed a similar impact of RGS7 knockdown in AC-16 cells on subsequent VCF activation (Fig. S8A–D). Finally, as RGS7 overexpression alone drives inflammatory cytokine production by VCM,

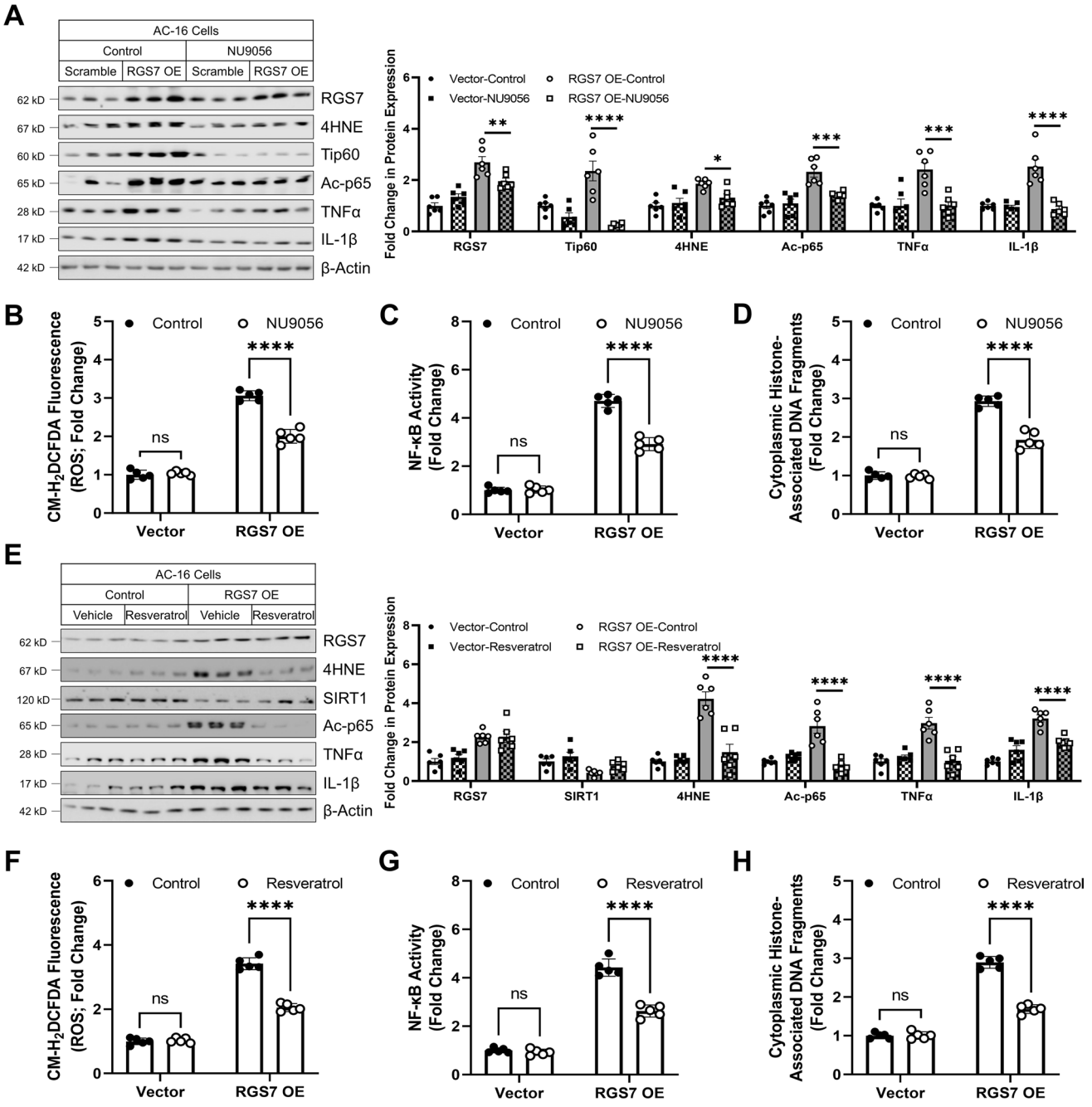

Fig. 5 Tip60 inhibition or SIRT1 activation prevents RGS7-dependent oxidative stress, inflammatory signaling, and cell loss in human cardiomyocytes. **A**–**D** AC-16 cells were transduced with vector control or RGS7-GFP (RGS7 overexpression, OE) ± Tip60 inhibitor NU 9056 (50 μM, 1 h pre-treatment) or vehicle control and harvested 36 h after transduced. **A** Immunoblotting for RGS7, 4HNE, Tip60, acetylated p65, TNFα, and IL-1β with quantification ($n=6$). **B** CM-H_2DCFDA fluorescence (ROS; $n=5$). **C** NF-kB activity ($n=5$). **D** Apoptosis (cytoplasmic histone-associated DNA fragments; ($n=5$). **E**–**H** AC-16 cells were transduced with vector control or RGS7-GFP (RGS7 overexpression, OE) ± SIRT1 activator resveratrol (20 μM, 4 h pre-treatment) or vehicle control and harvested 36 h after transduction. **E** Immunoblotting for RGS7, 4HNE, SIRT1, acetylated p65, TNFα, and IL-1β with quantification ($n=6$). **F** CM-H_2DCFDA fluorescence (ROS; $n=5$). **G** NF-kB activity ($n=5$). **H** Apoptosis (cytoplasmic histone-associated DNA fragments; ($n=5$). Data were analyzed by two-way ANOVA with Sidak's post hoc test. *$P<0.05$, **$P<0.01$, ***$P<0.001$, ****$P<0.0001$. *ns* not significant. Data are presented as mean ± SEM

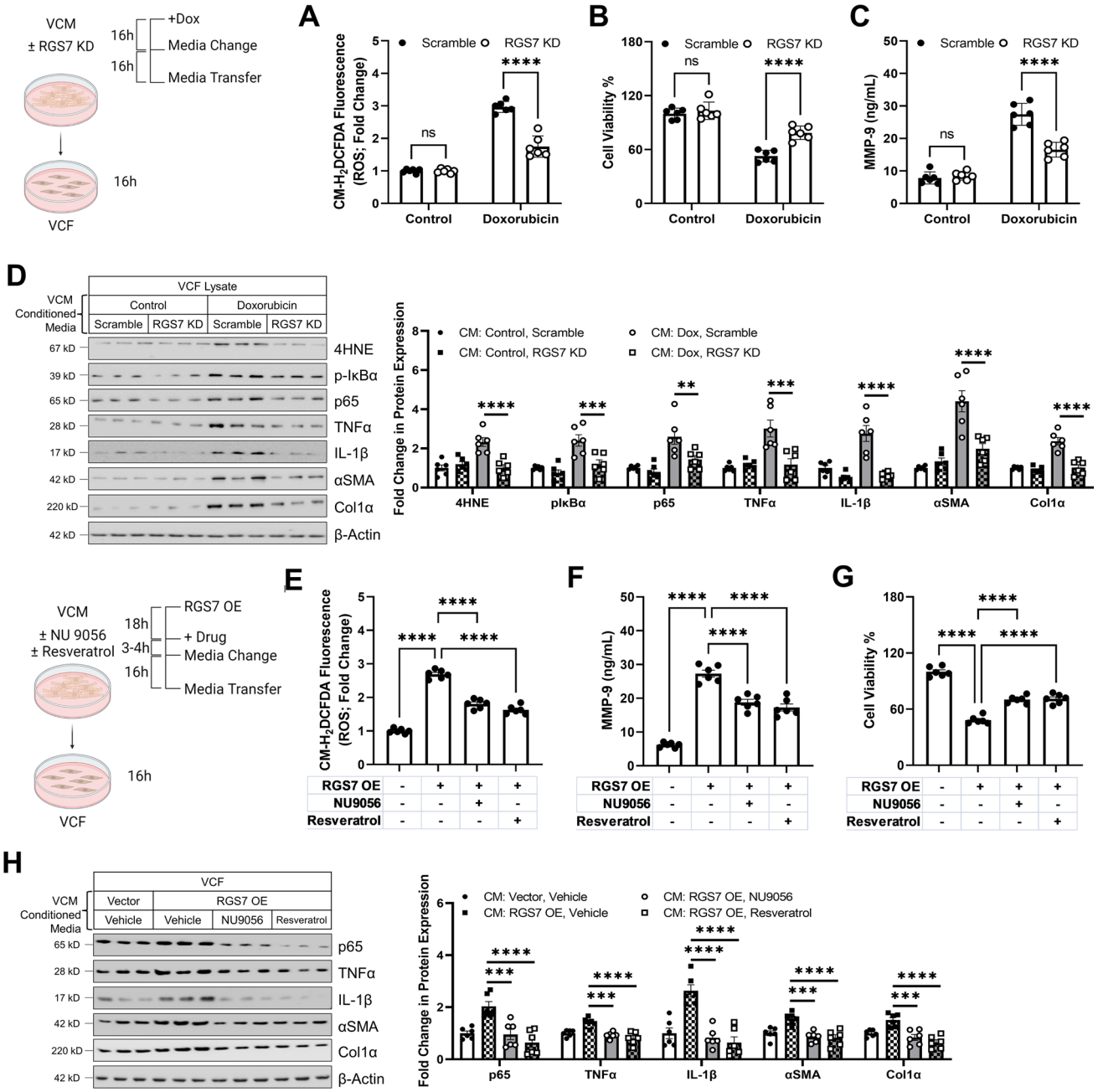

Fig. 6 RGS7 drives release of pro-inflammatory and pro-fibrotic factors from VCM via a mechanism involving Tip60 activation and SIRT1 inhibition. **A**–**D** Murine VCMs were transduced with scramble or RGS7-specific shRNA and treated with doxorubicin (3 μM, 16 h) 18 h after transduction. Media was replaced and 16 h later media was removed and added to VCF cultures for 16 h at which point VCF were harvested. **A** CM-H_2DCFDA fluorescence (ROS; $n=6$). **B** Cell viability as determined by MTT assay ($n=6$). **C** MMP-9 activity ($n=6$). **D** Immunoblotting for 4HNE, p-IκBα, p65, TNFα, IL-1β, αSMA, and Col1α with quantification ($n=6$). **E**–**H** Murine VCMs were transduced with RGS7 (RGS7 overexpression, OE) or vector control and treated with Tip60 inhibitor NU9056 (5 μM, 3 h treatment) or SIRT1 activator Resveratrol (20 μM, 4 h) 18 h after transduction. Media was replaced and 16 h later media was removed and added to VCF cultures for 16 h at which point VCF were harvested. **E** CM-H_2DCFDA fluorescence (ROS; $n=6$). **F** Cell viability as determined by MTT assay ($n=6$). **G** MMP-9 activity ($n=6$). **H** Immunoblotting for 4HNE, p-IκBα, p65, TNFα, IL-1β, αSMA, and Col1α with quantification ($n=6$). β-Actin serves as a loading control for immunoblots. Diagrams were created using Biorender.com. Data were analyzed by one- or two-way ANOVA with Sidak's post hoc test. $^{**}P<0.01$, $^{***}P<0.001$, $^{****}P<0.0001$. *ns* not significant. Data are presented as mean ± SEM

we were not surprised to note that, like doxorubicin, RGS7 overexpression in VCM triggered release of factors capable of driving oxidative stress (Fig. 6E), cell loss (Fig. 6F), MMP-9 activation (Fig. 6G), and pro-inflammatory and pro-fibrotic cytokine release (Fig. 6H) in VCF. Treatment of VCM with an inhibitor of TNFα prevented the increased oxidative stress (Fig. S8E), cell loss (Fig. S8F), MMP-9 activation (Fig. S8G), and accumulation of fibrotic and inflammatory factors (Fig. S8H) observed in VCF treated with conditioned media from VCM in which RGS7 was overexpressed. Thus, VCM releases TNFα in an RGS7-dependent manner that is capable of damaging neighboring VCF. Next, we wished to establish if modulation of protein acetylation would mitigate the detrimental VCM-VCF crosstalk driven by overexpression of RGS7 in VCM. Indeed, treatment of VCM with the Tip60 blocker NU9056 or SIRT1 activator resveratrol decreased oxidative stress (Fig. 6E), lessened MMP-9 activation (Fig. 6F), improved cell viability (Fig. 6G), and prevented production of inflammatory and fibrotic factors (Fig. 6H) in VCF that were exposed to media collected from VCM transfected with RGS7. These data demonstrated that the ability of RGS7 in VCM to promote VCF dysfunction requires, at least partially, a disruption in the relative activity of Tip60 and SIRT1.

Activation of sirtuins prevents RGS7-dependent cardiac inflammation in vivo

Finally, we wished to establish the relative importance of protein acetylation in the pro-inflammatory and pro-fibrotic actions of RGS7 in the heart. To do this, we introduced a viral vector for RGS7 overexpression into mice via intracardiac injection resulting in an approximately twofold increase in RGS7 expression in heart (Fig. 7A, B). As we observed in cultured cells, RGS7 overexpression in heart decreased SIRT1 expression (Fig. 7A, C), increased p65 acetylation (Fig. 7A, D), and triggered fibrosis (Fig. 7A, E). These histological changes were accompanied by increased protein levels of Tip60, phospho-IκBα, p65, TNFα, IL-1β, and 4HNE (Fig. S9) as well as increased oxidative stress (Fig. 7F). Remarkably, activation of sirtuins with resveratrol was sufficient to rescue or significantly mitigate the pro-inflammatory impacts of RGS7 overexpression on the heart

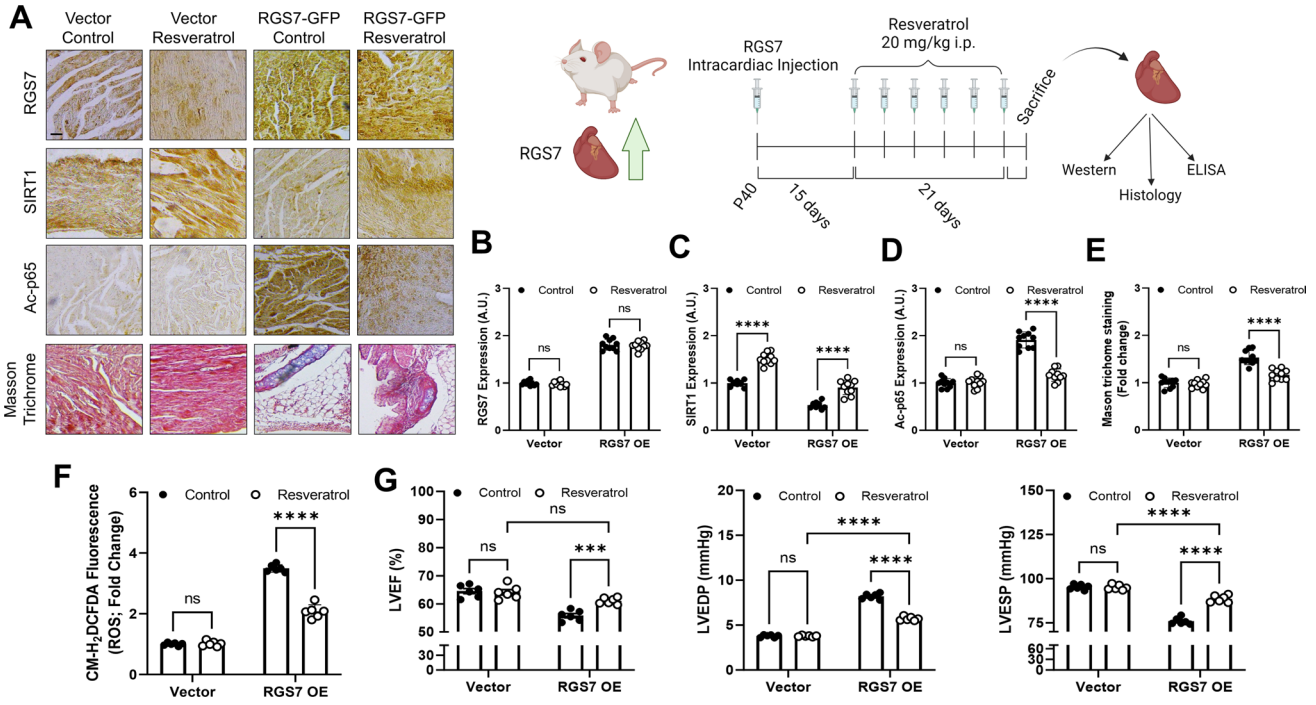

Fig. 7 RGS7-dependent cardiotoxicity can be mitigated by activating SIRT1. (A-H). An RGS7 encoding viral construct or vector control was introduced into the myocardium of mice (P40). After 15 days, animals were given DMSO (control) or resveratrol (20 mg/kg, i.p., two times per week) for 3 weeks at which point animals were euthanized and tissues collected for downstream analyses. **A** Representative images [scale bar = 100 μm] of RGS7, SIRT1, and acetyl-p65 expression and fibrosis (Masson Trichrome staining) in heart. Quantification of **B** RGS7; **C** SIRT1; **D** Acetyl p65 histoscores ($n = 10$). **E** Quantification of collagen deposition (Masson Trichrome, $n = 10$). **F** CM-H2DCFDA fluorescence (total ROS; $n = 6$). **G** Cardiac phenotyping for left-ventricular ejection fraction (LVEF), left-ventricular end-diastolic pressure (LVEDP), and left-ventricular end -systolic pressure (LVESP) ($n = 6$). β-Actin serves as a loading control for western blots. Diagram was created using Biorender.com. Data were analyzed by two-way ANOVA with Sidak's post hoc test. ***$P < 0.001$, ****$P < 0.0001$. *ns* not significant. Data are presented as mean ± SEM

(Figs. 7A–F, S9). Importantly, resveratrol treatment partially prevented the loss of left-ventricular function resulting from cardiac RGS7 overexpression (Fig. 7G). Together, these data indicate that RGS7-dependent suppression of sirtuin function drives cardiac inflammation and fibrosis and compromises cardiac function.

Discussion

Despite decades of research, the etiology of chemotherapy-dependent cardiotoxicity remains poorly defined. The current working theory posits that oxidant damage to cardiomyocytes initiates a cascade of autocrine and paracrine signaling events that, while initially aimed at clearing cellular detritus, remodeling the extracellular matrix, and filling gaps in the contractile apparatus to maintain cardiac output, becomes detrimental to cardiac function over time. Persistent sterile inflammation and release of inflammatory cytokines such as TNFα can lead to heart damage by disrupting calcium handling and triggering apoptosis in cardiomyocytes and promoting ongoing extracellular matrix degradation, excess collagen deposition, fibrosis, and hypertrophy [53]. Targeting immune mediators therapeutically represents a unique challenge due to the biphasic role of the innate immune system in cardiac disease. Here, we describe a role for RGS7 in amplification of maladaptive cardiac inflammation following exposure to the anthracycline chemotherapeutic doxorubicin. RGS7, whose expression is elevated in the hearts of patients with a history of chemotherapy, detectable fibrosis, and loss of ventricular function, forms a complex with the acetylase Tip60 and deacetylase SIRT1 in heart whose composition is influenced by doxorubicin such that chemotherapeutic exposure favors RGS7-Tip60 binding. Importantly, RGS7 expression is both necessary and sufficient to promote doxorubicin-dependent acetylation and activation of NF-κB subunit p65 and resultant production of pro-inflammatory cytokines from cardiomyocytes (Fig. 8). RGS7-dependent production of cytokines such as TNFα and IL-1β as well as chemoattractants such as MCP-1 would likely increase recruitment of immune cell types to the heart. Indeed, RGS7 knockdown in heart ameliorates doxorubicin-driven oxidative stress, inflammation, and fibrosis, while RGS7 overexpression triggers inflammatory cardiomyopathy via a mechanism requiring suppression of sirtuin function.

Simultaneous binding between RGS7 and two proteins, Tip60 and SIRT1, with diametrically opposed functions, is seemingly paradoxical especially given our molecular dynamics simulations heavily imply that the trimeric complex is more energetically favorable and results in closer

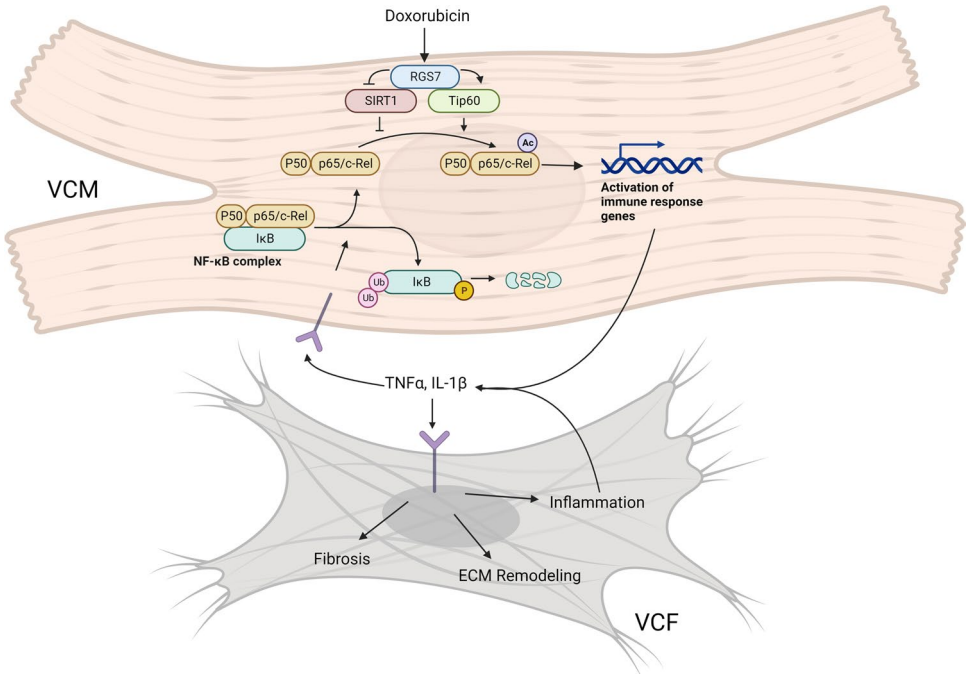

Fig. 8 Model depicting the role of RGS7 in doxorubicin-induced cardiac inflammation. Our data support a model wherein RGS7 forms a complex with SIRT1 and Tip60 in VCM. RGS7 suppresses the actions of deacetylase SIRT1 while simultaneously activating Tip60 leading to a net increase in acetylation of NF-κB subunit p65. Activated NF-κB drives release of inflammatory cytokines from damaged myocytes and stimulates transdifferentiation, extracellular matrix (ECM) remodeling, and collagen production in neighboring fibroblasts, which also contribute to accumulation of inflammatory mediators in the myocardium. In this way, RGS7 functions to amplify inflammatory signaling in heart and drive chemotherapy-induced cardiac fibrosis. The model was created using Biorender.com

intermolecular interactions as compared to a complex containing only RGS7 and Tip60. Indeed, our observation that Tip60 and SIRT1 binding is influenced by deletion of the same RGS7 domains (DEP and RGS) favors a model whereby binding of RGS7 to each protein is mutually exclusive. However, while doxorubicin treatment decreases the relative proportion of RGS7 complexes containing SIRT1 and increases those containing Tip60, this may simply be due to the relative abundance of each protein and not a doxorubicin-modulated state of RGS7. Functionally, RGS7 appears to facilitate Tip60 action while suppressing SIRT1 as the impact of RGS7 overexpression on ROS generation, NF-κB acetylation and activity, cytokine production, and apoptosis in myocytes can be mitigated via Tip60 inhibition or sirtuin activation. It remains unclear, however, how exactly RGS7 influences the activity of each protein, which could involve modulation of acetylase/deacetylase catalytic activity, subcellular localization, or substrate recruitment. The stability and activity of Tip60 are facilitated by autoacetylation at lysine 327 [54], a residue targeted by SIRT1 for deacetylation [55, 56] supporting a hierarchical model whereby RGS7 controls dynamic regulation of Tip60 by SIRT1, thereby gating acetylation of Tip60 substrates.

Studies describing a role for Tip60 in cardiac injury are sparse and confined to a demonstration of cardioprotective actions for Tip60 inhibition or gene deletion following myocardial infarction due to a decrease in cell death and enhanced regeneration [57, 58]. In contrast, several key SIRT1 targets have been identified in heart including the metabolic regulator peroxisome proliferator-activated receptor-gamma coactivator (PGC)-1α, tumor suppressor p53, and transcription factor nuclear factor-erythroid factor 2-related factor 2 (NRF2) [59]. Importantly, activation of SIRT1 decreases doxorubicin-dependent oxidative stress, cell death, and induction of inflammatory mediators such as TNFα [30–32]. Though prior reports investigated acetylation of NF-κB regulators including liver kinase B1 (LKB1) [32] following SIRT1 modulation, they failed to look directly at p65 acetylation. Normally sequestered in the cytoplasm by IκBα, the transcription factor NF-κB translocates to the nucleus following pro-inflammatory cytokine-dependent phosphorylation and degradation of IκBα [60]. NF-κB activity is also controlled via post-translational modifications and, notably, acetylation of p65 at lysine 310 is critical for full NF-κB transcriptional activity [61] and is an indirect and direct target of Tip60 [28] and SIRT1 [33], respectively. Tip60 can also directly bind to p65, and this interaction enhances NF-κB activity [28]. Neonatal and adult cardiomyocytes are resistant to the expression of pro-inflammatory genes due to impairment in the activation of IκB kinase [62] and overexpression of constitutively active IκB kinase in heart leads to inflammatory cardiomyopathy and heart failure [63, 64]. RGS7 overexpression in heart increased both phosphorylation of IκBα and acetylation of p65. Given that SIRT1 activation ameliorated both these impacts, it stands to reason that the impact of RGS7 on phospho-IκBα may be secondary to the reduction in cytokine production resulting from loss of p65 acetylation. This supposition is consistent with our observation that expression of p65 target genes, such as TNFα, IL-1β, and MCP-1 [65, 66], directly parallel RGS7 expression in heart. Thus, RGS7 functions in this context to prime NF-κB for maximal activation following autocrine or paracrine cytokine release. Such sustained p65 acetylation, facilitated by RGS7, would sensitize myocytes to the pro-apoptotic and pro-fibrotic actions of even low-level cytokine production and is likely detrimental to cardiac function providing a viable explanation for the high expression of RGS7 and acetylated p65 in the hearts of patients with a history of chemotherapy and heart failure.

In keeping with a model whereby RGS7 functions as an amplifier for inflammatory signaling, we and others have shown that TNFα increases RGS7 expression [24–26]. Though the exact mechanism remains unclear, TNFα does promote RGS7 phosphorylation at Ser 434, a reside in the RGS domain [26]. The deletion of the RGS domain decreases the RGS7/SIRT1 and RGS7/Tip60 interactions, and this residue was identified in our molecular dynamics simulation as involved in RGS7–Tip60 binding. Thus, it is possible that TNFα exposure may directly influence complex formation between RGS7 and Tip60/SIRT1 as has been demonstrated for 14-3-3/RGS7 binding [26]. TNFα production following doxorubicin exposure is also RGS7 dependent, and we found that RGS7-dependent release of pro-inflammatory cytokines from VCM was sufficient to induce oxidative stress, MMP-9 activation, and promote transdifferentiation of VCF. Thus, this cyclical relationship between RGS7 and TNFα likely functions to both magnify and propagate the impact of cardiac inflammation beyond the initial site of injury. We should note that the impact of RGS7 on inflammation may not be exclusively due to myocyte-intrinsic actions as RGS7 expression has also been detected in macrophages after immune challenge [67].

Several studies have demonstrated that increasing SIRT1 expression or activity protects against doxorubicin-induced cardiotoxicity by suppressing certain key targets including NF-κB [68, 69] but also the pro-apoptotic p53 [37, 70, 71] and p38 MAPK [39] as well as the pro-fibrotic TGF-β1 pathways [38]. In a prior study, we demonstrated that RGS7 promotes apoptosis in cardiac myocytes by increasing oxidative stress and impairing mitochondrial function, actions that involve a direct and functional interaction between RGS7 and the Ca^{2+}/calmodulin-dependent kinase CaMKII [23]. However, inhibition of CaMKII provided only partial protection against RGS7-dependent cardiotoxicity, indicating that RGS7 likely has additional effectors in the myocardium, a list that we now demonstrate includes SIRT1

and Tip60. What remains unclear is why a protein whose canonical role is in suppression of GPCR signaling at the cell membrane acts as a scaffold for cytosolic and nuclear signal transducers. In neurons, a palmitoylated accessory protein, R7 family-binding protein (R7BP), anchors R7 family RGS proteins at the membrane and regulates membrane/nuclear shuttling [72, 73], a process dependent on $G\alpha_{i/o}$ activity [74]. These data have underscored a prevailing hypothesis that RGS7 localization in nucleus is merely a means to sequester the protein away from the membrane where its GAP activity would be employed. However, R7BP is not expressed outside the nervous system [75]. Thus, in non-neuronal cell types, it is possible that a greater proportion of RGS7 may be present in the cytosol where it is free to interact with additional effectors. Expression of RGS7 is much lower in peripheral tissues as compared to the brain [76, 77]. However, in the presence of cytotoxic stressors such as doxorubicin [23] or a high-fat diet [24], RGS7 protein levels increase by several fold indicating two possible mechanisms underlying unique, non-G-protein-dependent actions of RGS7 in myocytes: dynamic regulation of RGS7 expression and a lack of membrane sequestration due to an absence of R7BP.

RGS7 is not the only R7 family member present in heart with RGS6 and RGS11 are also expressed at detectable levels [43, 78]. Intriguingly, while RGS6 and RGS7 expression increases in the myocardium in response to doxorubicin [23, 78], RGS11 decreases [43]. Like RGS7, RGS6 also promotes doxorubicin-dependent cardiac damage with RGS6 knockout providing marked protection against oxidative stress and cell death following doxorubicin exposure, actions attributed to direct binding of RGS6 to ATM [79] and regulation of the pro-apoptotic p53 signaling cascade [78]. RGS11, conversely, directly antagonizes the pro-apoptotic and pro-fibrotic actions of RGS7 in the doxorubicin-treated myocardium with RGS7 and RGS11 having directly antagonistic impacts on myocyte CaMKII activity [43]. As $G\beta_5$, a requisite, stabilizing binding partner of all R7 family members [80], is pro-apoptotic and pro-fibrotic [48], it is likely that RGS7 and RGS6 activity predominates in the presence of cytotoxic stress. Given that RGS6 and RGS7 share ~ 75% homology, it is surprising that they appear to control distinct signaling cascades in heart, though both are capable of binding to Tip60 [81]. Most notably, RGS6[82, 83], but not RGS7 [23], is pro-apoptotic and required for cytotoxic actions of doxorubicin in cancer cells. RGS6 is a potent tumor suppressor particularly in breast and bladder cancer, diseases whose therapeutic regimens often include an anthracycline [81, 83–85]. RGS6 also functions to limit parasympathetic drive by inhibiting G-protein-coupled muscarinic M2 receptors in cardiac pacemaker cells [86, 87] and RGS6 is associated with heart rate variability in both mice [88] and humans [89]. RGS7 inhibition, thus, would be expected to permit RGS11 accumulation and counteract doxorubicin-induced inflammation and fibrosis without compromising the therapeutic efficacy of doxorubicin, driving de novo carcinogenesis, or interfering with parasympathetic tone making it a particularly attractive target for treatment or prevention of doxorubicin-induced cardiotoxicity.

Conclusions

Together, our data demonstrate that RGS7 is both necessary and sufficient to drive chemotherapy-dependent cardiac inflammation, fibrotic remodeling, and cell loss in the heart. These actions of RGS7 are due, at least in part, to its ability to balance the acetylation status of p65, a key subunit of the ubiquitous pro-inflammatory mediator NF-κB. As RGS7 both drives inflammatory cytokine production and is up-regulated by cytokine signaling in myocytes, RGS7 acts as an amplifier of inflammation in the myocardium and also plays a key role in propagation of inflammatory signaling beyond the cardiomyocyte. We propose that, by inhibiting RGS7, it may be possible to achieve selective suppression of maladaptive and pathological inflammation driving cardiac dysfunction following exposure to cardiotoxic drugs.

Supplementary Information The online version contains supplementary material available at https://doi.org/10.1007/s00018-023-04895-5.

Acknowledgements The authors convey our sincere gratitude to DR. Sayan Biswas, MD, Assistant Professor, Department of Forensic Medicine, College of Medicine and Sagore Dutta Hospital, Kolkata, West Bengal for providing the human autopsy samples. The authors are thankful to Aryakul College of Pharmacy & Research, Lucknow for the help in mice experiments. Dr. Pranesh Kumar was appointed as Assistant Professor there before he moved to University of Lucknow.

Author contributions Conception and design: MB, AS, and BM. Acquisition of data: MB, KD, TM, DK, PK, NN, and KMP. Analysis and interpretation of data: MB, KD, TM, NN, KMP, PK, PD, and AS, BM. Writing or revision of the manuscript: MB, AS, and BM. Study supervision: AS and BM.

Funding We acknowledge funds from Indian Council of Medical Research (ICMR-5/4/1-26/2020-NCD-I and 5/4/1-22/CVD/2022-NCD-I) to BM.

Availability of data and materials All the data are mentioned either in the manuscript or in the supplement.

Declarations

Conflict of interest The authors declare no conflicts of interest.

Ethical approval and consent to participate Mouse experiments were performed at the Aryakul College of Pharmacy & Research, Lucknow, India under the guidance of Dr. Pranesh Kumar. Animals were procured

after obtaining clearance from the college Animal Ethics Committee (1896/PO/Re/S/16/CPCSEA/2021/5). Post-mortem human tissue samples were acquired from the Department of Forensic Medicine, Sagore Dutta Medical College & Hospital, Kolkata, West Bengal after obtaining the ethical clearance from the Centre of Biomedical Research Ethics Committee (Ref: IEC/CBMR/Corr/2020/16/6).

Consent for publication All the authors give their consent to publication.

References

1. Swain SM, Whaley FS, Ewer MS (2003) Congestive heart failure in patients treated with doxorubicin: a retrospective analysis of three trials. Cancer 97(11):2869–2879
2. Armenian SH, Hudson MM, Mulder RL, Chen MH, Constine LS, Dwyer M, Nathan PC, Tissing WJ, Shankar S, Sieswerda E, Skinner R, Steinberger J, van Dalen EC, van der Pal H, Wallace WH, Levitt G, Kremer LC, G International Late Effects of Childhood Cancer Guideline Harmonization (2015) Recommendations for cardiomyopathy surveillance for survivors of childhood cancer: a report from the International Late Effects of Childhood Cancer Guideline Harmonization Group. Lancet Oncol 16(3):e123–e136
3. Bures J, Jirkovska A, Sestak V, Jansova H, Karabanovich G, Roh J, Sterba M, Simunek T, Kovarikova P (2017) Investigation of novel dexrazoxane analogue JR-311 shows significant cardioprotective effects through topoisomerase IIbeta but not its iron chelating metabolite. Toxicology 392:1–10
4. Tebbi CK, London WB, Friedman D, Villaluna D, De Alarcon PA, Constine LS, Mendenhall NP, Sposto R, Chauvenet A, Schwartz CL (2007) Dexrazoxane-associated risk for acute myeloid leukemia/myelodysplastic syndrome and other secondary malignancies in pediatric Hodgkin's disease. J Clin Oncol 25(5):493–500
5. Henriksen PA (2018) Anthracycline cardiotoxicity: an update on mechanisms, monitoring and prevention. Heart 104(12):971–977
6. Cardinale D, Iacopo F, Cipolla CM (2020) Cardiotoxicity of anthracyclines. Front Cardiovasc Med 7:26
7. Minotti G, Menna P, Salvatorelli E, Cairo G, Gianni L (2004) Anthracyclines: molecular advances and pharmacologic developments in antitumor activity and cardiotoxicity. Pharmacol Rev 56(2):185–229
8. Childs AC, Phaneuf SL, Dirks AJ, Phillips T, Leeuwenburgh C (2002) Doxorubicin treatment in vivo causes cytochrome C release and cardiomyocyte apoptosis, as well as increased mitochondrial efficiency, superoxide dismutase activity, and Bcl-2:Bax ratio. Cancer Res 62(16):4592–4598
9. Davies KJ, Doroshow JH (1986) Redox cycling of anthracyclines by cardiac mitochondria. I. Anthracycline radical formation by NADH dehydrogenase. J Biol Chem 261(7):3060–3067
10. Doroshow JH, Davies KJ (1986) Redox cycling of anthracyclines by cardiac mitochondria. II. Formation of superoxide anion, hydrogen peroxide, and hydroxyl radical. J Biol Chem 261(7):3068–3074
11. Minotti G, Recalcati S, Menna P, Salvatorelli E, Corna G, Cairo G (2004) Doxorubicin cardiotoxicity and the control of iron metabolism: quinone-dependent and independent mechanisms. Methods Enzymol 378:340–361
12. Zhao Y, McLaughlin D, Robinson E, Harvey AP, Hookham MB, Shah AM, McDermott BJ, Grieve DJ (2010) Nox2 NADPH oxidase promotes pathologic cardiac remodeling associated with Doxorubicin chemotherapy. Cancer Res 70(22):9287–9297
13. Ma ZG, Kong CY, Wu HM, Song P, Zhang X, Yuan YP, Deng W, Tang QZ (2020) Toll-like receptor 5 deficiency diminishes doxorubicin-induced acute cardiotoxicity in mice. Theranostics 10(24):11013–11025
14. Guo Z, Tang N, Liu FY, Yang Z, Ma SQ, An P, Wu HM, Fan D, Tang QZ (2020) TLR9 deficiency alleviates doxorubicin-induced cardiotoxicity via the regulation of autophagy. J Cell Mol Med 24(18):10913–10923
15. Nozaki N, Shishido T, Takeishi Y, Kubota I (2004) Modulation of doxorubicin-induced cardiac dysfunction in toll-like receptor-2-knockout mice. Circulation 110(18):2869–2874
16. Riad A, Bien S, Gratz M, Escher F, Westermann D, Heimesaat MM, Bereswill S, Krieg T, Felix SB, Schultheiss HP, Kroemer HK, Tschope C (2008) Toll-like receptor-4 deficiency attenuates doxorubicin-induced cardiomyopathy in mice. Eur J Heart Fail 10(3):233–243
17. Krysko DV, Kaczmarek A, Krysko O, Heyndrickx L, Woznicki J, Bogaert P, Cauwels A, Takahashi N, Magez S, Bachert C, Vandenabeele P (2011) TLR-2 and TLR-9 are sensors of apoptosis in a mouse model of doxorubicin-induced acute inflammation. Cell Death Differ 18(8):1316–1325
18. Boyd JH, Mathur S, Wang Y, Bateman RM, Walley KR (2006) Toll-like receptor stimulation in cardiomyoctes decreases contractility and initiates an NF-kappaB dependent inflammatory response. Cardiovasc Res 72(3):384–393
19. Kaczmarek A, Krysko O, Heyndrickx L, Love-Aaes T, Delvaeye T, Bachert C, Leybaert L, Vandenabeele P, Krysko DV (2013) TNF/TNF-R1 pathway is involved in doxorubicin-induced acute sterile inflammation. Cell Death Dis 4(12):e961
20. Bhagat A, Shrestha P, Jeyabal P, Peng Z, Watowich SS, Kleinerman ES (2022) Doxorubicin-induced cardiotoxicity is mediated by neutrophils through release of neutrophil elastase. Front Oncol 12:947604
21. Zhang H, Xu A, Sun X, Yang Y, Zhang L, Bai H, Ben J, Zhu X, Li X, Yang Q, Wang Z, Wu W, Yang D, Zhang Y, Xu Y, Chen Q (2020) Self-maintenance of cardiac resident reparative macrophages attenuates doxorubicin-induced cardiomyopathy through the SR-A1-c-Myc axis. Circ Res 127(5):610–627
22. Clayton ZS, Brunt VE, Hutton DA, Casso AG, Ziemba BP, Melov S, Campisi J, Seals DR (2021) Tumor necrosis factor alpha-mediated inflammation and remodeling of the extracellular matrix underlies aortic stiffening induced by the common chemotherapeutic agent doxorubicin. Hypertension 77(5):1581–1590
23. Basak M, Sengar AS, Das K, Mahata T, Kumar M, Kumar D, Biswas S, Sarkar S, Kumar P, Das P, Stewart A, Maity B (2023) A RGS7-CaMKII complex drives myocyte-intrinsic and myocyte-extrinsic mechanisms of chemotherapy-induced cardiotoxicity. Proc Natl Acad Sci U S A 120(1):e2213537120
24. Basak M, Das K, Mahata T, Sengar AS, Verma SK, Biswas S, Bhadra K, Stewart A, Maity B (2023) RGS7-ATF3-Tip60 complex promotes hepatic steatosis and fibrosis by directly inducing TNFalpha. Antioxid Redox Signal 38(1–3):137–159
25. Benzing T, Brandes R, Sellin L, Schermer B, Lecker S, Walz G, Kim E (1999) Upregulation of RGS7 may contribute to tumor necrosis factor-induced changes in central nervous function. Nat Med 5(8):913–918
26. Benzing T, Kottgen M, Johnson M, Schermer B, Zentgraf H, Walz G, Kim E (2002) Interaction of 14-3-3 protein with regulator of G protein signaling 7 is dynamically regulated by tumor necrosis factor-alpha. J Biol Chem 277(36):32954–32962
27. Zhang JH, Barr VA, Mo Y, Rojkova AM, Liu S, Simonds WF (2001) Nuclear localization of G protein beta 5 and regulator of G protein signaling 7 in neurons and brain. J Biol Chem 276(13):10284–10289
28. Kim JW, Jang SM, Kim CH, An JH, Kang EJ, Choi KH (2012) New molecular bridge between RelA/p65 and NF-kappaB target

genes via histone acetyltransferase TIP60 cofactor. J Biol Chem 287(10):7780–7791
29. Greene WC, Chen LF (2004) Regulation of NF-kappaB action by reversible acetylation. Novartis Found Symp 259:208–217 (**discussion 218–25**)
30. Kuno A, Hosoda R, Tsukamoto M, Sato T, Sakuragi H, Ajima N, Saga Y, Tada K, Taniguchi Y, Iwahara N, Horio Y (2023) SIRT1 in the cardiomyocyte counteracts doxorubicin-induced cardiotoxicity via regulating histone H2AX. Cardiovasc Res 118(17):3360–3373
31. Yuan YP, Ma ZG, Zhang X, Xu SC, Zeng XF, Yang Z, Deng W, Tang QZ (2018) CTRP3 protected against doxorubicin-induced cardiac dysfunction, inflammation and cell death via activation of Sirt1. J Mol Cell Cardiol 114:38–47
32. Wang S, Wang Y, Zhang Z, Liu Q, Gu J (2017) Cardioprotective effects of fibroblast growth factor 21 against doxorubicin-induced toxicity via the SIRT1/LKB1/AMPK pathway. Cell Death Dis 8(8):e3018
33. Yeung F, Hoberg JE, Ramsey CS, Keller MD, Jones DR, Frye RA, Mayo MW (2004) Modulation of NF-kappaB-dependent transcription and cell survival by the SIRT1 deacetylase. EMBO J 23(12):2369–2380
34. Moulin M, Piquereau J, Mateo P, Fortin D, Rucker-Martin C, Gressette M, Lefebvre F, Gresikova M, Solgadi A, Veksler V, Garnier A, Ventura-Clapier R (2015) Sexual dimorphism of doxorubicin-mediated cardiotoxicity: potential role of energy metabolism remodeling. Circ Heart Fail 8(1):98–108
35. Nair A, Morsy MA, Jacob S (2018) Dose translation between laboratory animals and human in preclinical and clinical phases of drug development. Drug Dev Res 79(8):373–382
36. Nagai K, Nogami S, Egusa H, Konishi H (2014) Pharmacokinetic evaluation of intraperitoneal doxorubicin in rats. Pharmazie 69(2):125–127
37. Zhang C, Feng Y, Qu S, Wei X, Zhu H, Luo Q, Liu M, Chen G, Xiao X (2011) Resveratrol attenuates doxorubicin-induced cardiomyocyte apoptosis in mice through SIRT1-mediated deacetylation of p53. Cardiovasc Res 90(3):538–545
38. Cappetta D, Esposito G, Piegari E, Russo R, Ciuffreda LP, Rivellino A, Berrino L, Rossi F, De Angelis A, Urbanek K (2016) SIRT1 activation attenuates diastolic dysfunction by reducing cardiac fibrosis in a model of anthracycline cardiomyopathy. Int J Cardiol 205:99–110
39. Ruan Y, Dong C, Patel J, Duan C, Wang X, Wu X, Cao Y, Pu L, Lu D, Shen T, Li J (2015) SIRT1 suppresses doxorubicin-induced cardiotoxicity by regulating the oxidative stress and p38MAPK pathways. Cell Physiol Biochem 35(3):1116–1124
40. Pramanick A, Chakraborti S, Mahata T, Basak M, Das K, Verma SK, Sengar AS, Singh PK, Kumar P, Bhattacharya B, Biswas S, Pal PB, Sarkar S, Agrawal V, Saha S, Nath D, Chatterjee S, Stewart A, Maity B (2021) G protein beta5-ATM complexes drive acetaminophen-induced hepatotoxicity. Redox Biol 43:101965
41. Long CS, Henrich CJ, Simpson PC (1991) A growth factor for cardiac myocytes is produced by cardiac nonmyocytes. Cell Regul 2(12):1081–1095
42. Maillet A, Tan K, Chai X, Sadananda SN, Mehta A, Ooi J, Hayden MR, Pouladi MA, Ghosh S, Shim W, Brunham LR (2016) Modeling doxorubicin-induced cardiotoxicity in human pluripotent stem cell derived-cardiomyocytes. Sci Rep 6:25333
43. Das K, Basak M, Mahata T, Kumar M, Kumar D, Biswas S, Chatterjee S, Moniruzzaman M, Saha NC, Mondal K, Kumar P, Das P, Stewart A, Maity B (2022) RGS11-CaMKII complex mediated redox control attenuates chemotherapy-induced cardiac fibrosis. Redox Biol 57:102487
44. Liu MH, Shan J, Li J, Zhang Y, Lin XL (2016) Resveratrol inhibits doxorubicin-induced cardiotoxicity via sirtuin 1 activation in H9c2 cardiomyocytes. Exp Ther Med 12(2):1113–1118
45. Danz ED, Skramsted J, Henry N, Bennett JA, Keller RS (2009) Resveratrol prevents doxorubicin cardiotoxicity through mitochondrial stabilization and the Sirt1 pathway. Free Radic Biol Med 46(12):1589–1597
46. Coffey K, Blackburn TJ, Cook S, Golding BT, Griffin RJ, Hardcastle IR, Hewitt L, Huberman K, McNeill HV, Newell DR, Roche C, Ryan-Munden CA, Watson A, Robson CN (2012) Characterisation of a Tip60 specific inhibitor, NU9056, in prostate cancer. PLoS ONE 7(10):e45539
47. Pourtaghi-Anvarian S, Mohammadi S, Hamzeh-Mivehroud M, Alizadeh AA, Dastmalchi S (2019) Characterization of the novel anti-TNF-alpha single-chain fragment antibodies using experimental and computational approaches. Prep Biochem Biotechnol 49(1):38–47
48. Chakraborti S, Pramanick A, Saha S, Roy SS, Chaudhuri AR, Das M, Ghosh S, Stewart A, Maity B (2018) Atypical G protein beta5 promotes cardiac oxidative stress, apoptosis, and fibrotic remodeling in response to multiple cancer chemotherapeutics. Cancer Res 78(2):528–541
49. Kalyanaraman B, Darley-Usmar V, Davies KJ, Dennery PA, Forman HJ, Grisham MB, Mann GE, Moore K, Roberts LJ 2nd, Ischiropoulos H (2012) Measuring reactive oxygen and nitrogen species with fluorescent probes: challenges and limitations. Free Radic Biol Med 52(1):1–6
50. Pierce BG, Hourai Y, Weng Z (2011) Accelerating protein docking in ZDOCK using an advanced 3D convolution library. PLoS ONE 6(9):e24657
51. Negi SS, Schein CH, Oezguen N, Power TD, Braun W (2007) InterProSurf: a web server for predicting interacting sites on protein surfaces. Bioinformatics 23(24):3397–3399
52. Bozkurt B, Coats AJS, Tsutsui H, Abdelhamid CM, Adamopoulos S, Albert N, Anker SD, Atherton J, Bohm M, Butler J, Drazner MH, Michael Felker G, Filippatos G, Fiuzat M, Fonarow GC, Gomez-Mesa JE, Heidenreich P, Imamura T, Jankowska EA, Januzzi J, Khazanie P, Kinugawa K, Lam CSP, Matsue Y, Metra M, Ohtani T, Francesco Piepoli M, Ponikowski P, Rosano GMC, Sakata Y, Seferovic P, Starling RC, Teerlink JR, Vardeny O, Yamamoto K, Yancy C, Zhang J, Zieroth S (2021) Universal definition and classification of heart failure: a report of the Heart Failure Society of America, Heart Failure Association of the European Society of Cardiology, Japanese Heart Failure Society and Writing Committee of the Universal Definition of Heart Failure: Endorsed by the Canadian Heart Failure Society, Heart Failure Association of India, Cardiac Society of Australia and New Zealand, and Chinese Heart Failure Association. Eur J Heart Fail 23(3):352–380
53. Bhagat A, Shrestha P, Kleinerman ES (2022) The innate immune system in cardiovascular diseases and its role in doxorubicin-induced cardiotoxicity. Int J Mol Sci 23(23):14649
54. Xiao Y, Nagai Y, Deng G, Ohtani T, Zhu Z, Zhou Z, Zhang H, Ji MQ, Lough JW, Samanta A, Hancock WW, Greene MI (2014) Dynamic interactions between TIP60 and p300 regulate FOXP3 function through a structural switch defined by a single lysine on TIP60. Cell Rep 7(5):1471–1480
55. Wang J, Chen J (2010) SIRT1 regulates autoacetylation and histone acetyltransferase activity of TIP60. J Biol Chem 285(15):11458–11464
56. Yamagata K, Kitabayashi I (2009) Sirt1 physically interacts with Tip60 and negatively regulates Tip60-mediated acetylation of H2AX. Biochem Biophys Res Commun 390(4):1355–1360
57. Wang X, Wan TC, Kulik KR, Lauth A, Smith BC, Lough JW, Auchampach JA (2023) Pharmacological inhibition of the acetyltransferase Tip60 mitigates myocardial infarction injury. Dis Model Mech 16(5):049786
58. Wang X, Wan TC, Lauth A, Purdy AL, Kulik KR, Patterson M, Lough JW, Auchampach JA (2022) Conditional depletion of the

acetyltransferase Tip60 protects against the damaging effects of myocardial infarction. J Mol Cell Cardiol 163:9–19
59. Wang AJ, Zhang J, Xiao M, Wang S, Wang BJ, Guo Y, Tang Y, Gu J (2021) Molecular mechanisms of doxorubicin-induced cardiotoxicity: novel roles of sirtuin 1-mediated signaling pathways. Cell Mol Life Sci 78(7):3105–3125
60. Viatour P, Merville MP, Bours V, Chariot A (2005) Phosphorylation of NF-kappaB and IkappaB proteins: implications in cancer and inflammation. Trends Biochem Sci 30(1):43–52
61. Chen LF, Mu Y, Greene WC (2002) Acetylation of RelA at discrete sites regulates distinct nuclear functions of NF-kappaB. EMBO J 21(23):6539–6548
62. Goren N, Cuenca J, Martin-Sanz P, Bosca L (2004) Attenuation of NF-kappaB signalling in rat cardiomyocytes at birth restricts the induction of inflammatory genes. Cardiovasc Res 64(2):289–297
63. Kraut B, Maier HJ, Kokai E, Fiedler K, Boettger T, Illing A, Kostin S, Walther P, Braun T, Wirth T (2015) Cardiac-specific activation of IKK2 leads to defects in heart development and embryonic lethality. PLoS ONE 10(11):e0141591
64. Maier HJ, Schips TG, Wietelmann A, Kruger M, Brunner C, Sauter M, Klingel K, Bottger T, Braun T, Wirth T (2012) Cardiomyocyte-specific IkappaB kinase (IKK)/NF-kappaB activation induces reversible inflammatory cardiomyopathy and heart failure. Proc Natl Acad Sci U S A 109(29):11794–11799
65. Cheng W, Cui C, Liu G, Ye C, Shao F, Bagchi AK, Mehta JL, Wang X (2023) NF-kappaB, a potential therapeutic target in cardiovascular diseases. Cardiovasc Drugs Ther 37(3):571–584
66. Ueda A, Ishigatsubo Y, Okubo T, Yoshimura T (1997) Transcriptional regulation of the human monocyte chemoattractant protein-1 gene. Cooperation of two NF-kappaB sites and NF-kappaB/Rel subunit specificity. J Biol Chem 272(49):31092–31099
67. Hausmann ON, Hu WH, Keren-Raifman T, Witherow DS, Wang Q, Levay K, Frydel B, Slepak ZV, Bethea RJ (2002) Spinal cord injury induces expression of RGS7 in microglia/macrophages in rats. Eur J Neurosci 15(4):602–612
68. Lin B, Zhao H, Li L, Zhang Z, Jiang N, Yang X, Zhang T, Lian B, Liu Y, Zhang C, Wang J, Wang F, Feng D, Xu J (2020) Sirt1 improves heart failure through modulating the NF-kappaB p65/microRNA-155/BNDF signaling cascade. Aging (Albany NY) 13(10):14482–14498
69. Wang AJ, Tang Y, Zhang J, Wang BJ, Xiao M, Lu G, Li J, Liu Q, Guo Y, Gu J (2022) Cardiac SIRT1 ameliorates doxorubicin-induced cardiotoxicity by targeting sestrin 2. Redox Biol 52:102310
70. Sin TK, Tam BT, Yung BY, Yip SP, Chan LW, Wong CS, Ying M, Rudd JA, Siu PM (2015) Resveratrol protects against doxorubicin-induced cardiotoxicity in aged hearts through the SIRT1-USP7 axis. J Physiol 593(8):1887–1899
71. Xiao M, Tang Y, Wang J, Lu G, Niu J, Wang J, Li J, Liu Q, Wang Z, Huang Z, Guo Y, Gao T, Zhang X, Yue S, Gu J (2022) A new FGF1 variant protects against adriamycin-induced cardiotoxicity via modulating p53 activity. Redox Biol 49:102219
72. Drenan RM, Doupnik CA, Boyle MP, Muglia LJ, Huettner JE, Linder ME, Blumer KJ (2005) Palmitoylation regulates plasma membrane-nuclear shuttling of R7BP, a novel membrane anchor for the RGS7 family. J Cell Biol 169(4):623–633
73. Panicker LM, Zhang JH, Posokhova E, Gastinger MJ, Martemyanov KA, Simonds WF (2010) Nuclear localization of the G protein beta 5/R7-regulator of G protein signaling protein complex is dependent on R7 binding protein. J Neurochem 113(5):1101–1112
74. Jia L, Linder ME, Blumer KJ (2011) Gi/o signaling and the palmitoyltransferase DHHC2 regulate palmitate cycling and shuttling of RGS7 family-binding protein. J Biol Chem 286(15):13695–13703
75. Martemyanov KA, Yoo PJ, Skiba NP, Arshavsky VY (2005) R7BP, a novel neuronal protein interacting with RGS proteins of the R7 family. J Biol Chem 280(7):5133–5136
76. Larminie C, Murdock P, Walhin JP, Duckworth M, Blumer KJ, Scheideler MA, Garnier M (2004) Selective expression of regulators of G-protein signaling (RGS) in the human central nervous system. Brain Res Mol Brain Res 122(1):24–34
77. Kardestuncer T, Wu H, Lim AL, Neer EJ (1998) Cardiac myocytes express mRNA for ten RGS proteins: changes in RGS mRNA expression in ventricular myocytes and cultured atria. FEBS Lett 438(3):285–288
78. Yang J, Maity B, Huang J, Gao Z, Stewart A, Weiss RM, Anderson ME, Fisher RA (2013) G-protein inactivator RGS6 mediates myocardial cell apoptosis and cardiomyopathy caused by doxorubicin. Cancer Res 73(6):1662–1667
79. Mahata T, Sengar AS, Basak M, Das K, Pramanick A, Verma SK, Singh PK, Biswas S, Sarkar S, Saha S, Chatterjee S, Das M, Stewart A, Maity B (2021) Hepatic regulator of G protein signaling 6 (RGS6) drives non-alcoholic fatty liver disease by promoting oxidative stress and ATM-dependent cell death. Redox Biol 46:102105
80. Chen CK, Eversole-Cire P, Zhang H, Mancino V, Chen YJ, He W, Wensel TG, Simon MI (2003) Instability of GGL domain-containing RGS proteins in mice lacking the G protein beta-subunit Gbeta5. Proc Natl Acad Sci U S A 100(11):6604–6609
81. Huang J, Stewart A, Maity B, Hagen J, Fagan RL, Yang J, Quelle DE, Brenner C, Fisher RA (2014) RGS6 suppresses Ras-induced cellular transformation by facilitating Tip60-mediated Dnmt1 degradation and promoting apoptosis. Oncogene 33(27):3604–3611
82. Huang J, Yang J, Maity B, Mayuzumi D, Fisher RA (2011) Regulator of G protein signaling 6 mediates doxorubicin-induced ATM and p53 activation by a reactive oxygen species-dependent mechanism. Cancer Res 71(20):6310–6319
83. Maity B, Yang J, Huang J, Askeland RW, Bera S, Fisher RA (2011) Regulator of G protein signaling 6 (RGS6) induces apoptosis via a mitochondrial-dependent pathway not involving its GTPase-activating protein activity. J Biol Chem 286(2):1409–1419
84. Maity B, Stewart A, O'Malley Y, Askeland RW, Sugg SL, Fisher RA (2013) Regulator of G protein signaling 6 is a novel suppressor of breast tumor initiation and progression. Carcinogenesis 34(8):1747–1755
85. Yang J, Platt LT, Maity B, Ahlers KE, Luo Z, Lin Z, Chakravarti B, Ibeawuchi SR, Askeland RW, Bondaruk J, Czerniak BA, Fisher RA (2016) RGS6 is an essential tumor suppressor that prevents bladder carcinogenesis by promoting p53 activation and DNMT1 downregulation. Oncotarget 7(43):69159–69172
86. Yang J, Huang J, Maity B, Gao Z, Lorca RA, Gudmundsson H, Li J, Stewart A, Swaminathan PD, Ibeawuchi SR, Shepherd A, Chen CK, Kutschke W, Mohler PJ, Mohapatra DP, Anderson ME, Fisher RA (2010) RGS6, a modulator of parasympathetic activation in heart. Circ Res 107(11):1345–1349
87. Posokhova E, Wydeven N, Allen KL, Wickman K, Martemyanov KA (2010) RGS6/Gbeta5 complex accelerates IKACh gating kinetics in atrial myocytes and modulates parasympathetic regulation of heart rate. Circ Res 107(11):1350–1354
88. Posokhova E, Ng D, Opel A, Masuho I, Tinker A, Biesecker LG, Wickman K, Martemyanov KA (2013) Essential role of the m2R-RGS6-IKACh pathway in controlling intrinsic heart rate variability. PLoS ONE 8(10):e76973
89. Nolte IM, Munoz ML, Tragante V, Amare AT, Jansen R, Vaez A, von der Heyde B, Avery CL, Bis JC, Dierckx B, van Dongen J, Gogarten SM, Goyette P, Hernesniemi J, Huikari V, Hwang SJ, Jaju D, Kerr KF, Kluttig A, Krijthe BP, Kumar J, van der Laan SW, Lyytikainen LP, Maihofer AX, Minassian A, van der Most PJ, Muller-Nurasyid M, Nivard M, Salvi E, Stewart JD, Thayer JF, Verweij N, Wong A, Zabaneh D, Zafarmand MH, Abdellaoui A, Albarwani S, Albert C, Alonso A, Ashar F, Auvinen J, Axelsson T, Baker DG, de Bakker PIW, Barcella M, Bayoumi R, Bieringa RJ, Boomsma D, Boucher G, Britton AR, Christophersen I,

Dietrich A, Ehret GB, Ellinor PT, Eskola M, Felix JF, Floras JS, Franco OH, Friberg P, Gademan MGJ, Geyer MA, Giedraitis V, Hartman CA, Hemerich D, Hofman A, Hottenga JJ, Huikuri H, Hutri-Kahonen N, Jouven X, Junttila J, Juonala M, Kiviniemi AM, Kors JA, Kumari M, Kuznetsova T, Laurie CC, Lefrandt JD, Li Y, Li Y, Liao D, Limacher MC, Lin HJ, Lindgren CM, Lubitz SA, Mahajan A, McKnight B, Zu Schwabedissen HM, Milaneschi Y, Mononen N, Morris AP, Nalls MA, Navis G, Neijts M, Nikus K, North KE, O'Connor DT, Ormel J, Perz S, Peters A, Psaty BM, Raitakari OT, Risbrough VB, Sinner MF, Siscovick D, Smit JH, Smith NL, Soliman EZ, Sotoodehnia N, Staessen JA, Stein PK, Stilp AM, Stolarz-Skrzypek K, Strauch K, Sundstrom J, Swenne CA, Syvanen AC, Tardif JC, Taylor KD, Teumer A, Thornton TA, Tinker LE, Uitterlinden AG, van Setten J, Voss A, Waldenberger M, Wilhelmsen KC, Willemsen G, Wong Q, Zhang ZM, Zonderman AB, Cusi D, Evans MK, Greiser HK, van der Harst P, Hassan M, Ingelsson E, Jarvelin MR, Kaab S, Kahonen M, Kivimaki M, Kooperberg C, Kuh D, Lehtimaki T, Lind L, Nievergelt CM, O'Donnell CJ, Oldehinkel AJ, Penninx B, Reiner AP, Riese H, van Roon AM, Rioux JD, Rotter JI, Sofer T, Stricker BH, Tiemeier H, Vrijkotte TGM, Asselbergs FW, Brundel B, Heckbert SR, Whitsel EA, den Hoed M, Snieder H, de Geus EJC (2017) Genetic loci associated with heart rate variability and their effects on cardiac disease risk. Nat Commun 8:15805